

JGR Solid Earth

RESEARCH ARTICLE

10.1029/2022JB025135

Key Points:

- Mg and Zn isotopic decoupling is reported for the first time in circum-Mediterranean K-rich lavas
- Carbonate-bearing silicate sediments have been recycled into the lithospheric mantle beneath the circum-Mediterranean region
- Carbon-rich lithospheric mantle is an important source for extensive volcanic CO₂ emissions

Supporting Information:

Supporting Information may be found in the online version of this article.

Correspondence to:

S.-A. Liu,
lsa@cugb.edu.cn

Citation:

Shu, Z.-T., Liu, S.-A., Prelević, D., Wang, Y., Foley, S. F., Cvetković, V., & Li, S. (2023). Recycled carbonate-bearing silicate sediments in the sources of circum-Mediterranean K-rich lavas: Evidence from Mg-Zn isotopic decoupling. *Journal of Geophysical Research: Solid Earth*, 128, e2022JB025135. <https://doi.org/10.1029/2022JB025135>






Received 7 JUL 2022

Accepted 11 FEB 2023

Author Contributions:

Project Administration: Shuguang Li
Supervision: Sheng-Ao Liu, Stephen F. Foley, Shuguang Li
Writing – original draft: Zi-Tan Shu
Writing – review & editing: Sheng-Ao Liu, Dejan Prelević, Yu Wang, Stephen F. Foley, Vladica Cvetković, Shuguang Li

Recycled Carbonate-Bearing Silicate Sediments in the Sources of Circum-Mediterranean K-Rich Lavas: Evidence From Mg-Zn Isotopic Decoupling

Zi-Tan Shu¹ , Sheng-Ao Liu¹ , Dejan Prelević^{2,3} , Yu Wang⁴ , Stephen F. Foley⁵ , Vladica Cvetković³, and Shuguang Li¹

¹State Key Laboratory of Geological Processes and Mineral Resources, China University of Geosciences, Beijing, China,

²Institute of Geological Sciences, University of Mainz, Mainz, Germany, ³Faculty of Mining and Geology, University of Belgrade, Belgrade, Serbia, ⁴State Key Laboratory of Isotope Geochemistry, Guangzhou Institute of Geochemistry, Chinese Academy of Sciences, Guangzhou, China, ⁵School of Natural Sciences, Macquarie University, North Ryde, NSW, Australia

Abstract The high flux of subaerial volcanic CO₂ emissions around the circum-Mediterranean region requires the involvement of an unusually carbon-rich reservoir, but the origin of which is still unclear. Here, we aim to resolve this problem by analyzing Mg and Zn isotopes for the widely distributed mafic potassic to ultrapotassic lavas in this region. These K-rich lavas have lower $\delta^{26}\text{Mg}$ but similar $\delta^{66}\text{Zn}$ compared to mid-ocean ridge basalts (MORB). No known magmatic processes can explain the isotopic data, which must therefore be characteristics of the mantle sources. Recycled carbonate sediments are capable of explaining the low $\delta^{26}\text{Mg}$, but they typically also have high $\delta^{66}\text{Zn}$. Thus, the low $\delta^{26}\text{Mg}$ but unfractionated $\delta^{66}\text{Zn}$ of these K-rich lavas define “Mg-Zn isotopic decoupling” which has not yet been observed for other types of mantle-derived lavas. The carbonate-bearing silicate sediments analyzed here possess low $\delta^{26}\text{Mg}$ and MORB-like $\delta^{66}\text{Zn}$, which can account for the Mg-Zn isotopic decoupling. Therefore, the nature of recycled materials (carbonates vs. carbonate-bearing silicate sediments) in the mantle can be distinguished by the coupling or decoupling of Mg and Zn isotopes of mantle-derived magmas. The input flux of carbon from the sediments to the lithospheric mantle is estimated to be ~ 8.1 Mt/yr, and ~ 22.4 Mt/yr of CO₂ emissions are predicted, which fit well with the observed output flux of 20.1 ± 13.4 Mt/yr. Our results demonstrate that recycled crustal carbon stored in the lithospheric mantle is an important source for the extensive subaerial volcanic CO₂ emissions in the circum-Mediterranean region.

Plain Language Summary Extensive volcanic CO₂ emissions around the circum-Mediterranean region constitute a significant proportion of the global total, but the source of this carbon-rich reservoir is unclear. We analyze Mg and Zn isotopes for the widespread, lithospheric mantle-derived K-rich lavas in this region and find that they have lower Mg but similar Zn isotopic data compared to mid-ocean ridge basalts. This Mg-Zn isotopic feature is defined as “Mg-Zn isotopic decoupling” and explained as resulting from recycled carbonate-bearing sediments in their mantle sources. Thus, the lithospheric mantle beneath the circum-Mediterranean region is carbon-rich, providing an important source for the extensive volcanic CO₂ emissions.

1. Introduction

The solid Earth contains more carbon than the entire surface reservoir (ocean, atmosphere, and biosphere) in terms of mass: over 90% of carbon is located in the crust, mantle, and core (Dasgupta & Hirschmann, 2010; Wood, 1993). Carbon is released from the Earth's interior mainly in the form of carbon dioxide (CO₂) by degassing from volcanoes (up to 90%) and metamorphic reactions ($\approx 10\%$; Mason et al., 2017). The flux of CO₂ released from oceanic volcanism (mid-ocean ridges and ocean islands) is ~ 29 – 154 Megatons per year (Mt/yr) (Kelemen & Manning, 2015), and the global flux of CO₂ emitted from other volcanic environment, including plume degassing and diffuse degassing, is up to ~ 108 Mt/yr (Werner et al., 2019), which has a significant time-integrated impact on the concentration of atmospheric CO₂ (161×10^3 Mt; Lee et al., 2019). The circum-Mediterranean region, which experienced a prolonged period of convergence between the African-Arabian and the Eurasian plates from the late Jurassic to Cenozoic (Prelević & Foley, 2007), contributes an anomalously large flux of subaerial volcanic CO₂ emissions (20.1 Mt/yr; Werner et al., 2019), accounting for about 20% of the global total. This

enormous CO₂ output flux appears to require an extremely carbon-rich reservoir in the crust or mantle. It has been proposed that CO₂ emissions by arc volcanoes are largely sourced from subducting crustal carbon (>70%; Plank & Manning, 2019). However, there is no explanation so far for the high carbon flux in the circum-Mediterranean region.

Mantle-derived lavas are regarded as an ideal proxy to link volcanic CO₂ outgassing with deep carbon cycling (e.g., Avanzinelli et al., 2018; Bragagni et al., 2022). The circum-Mediterranean region is well-known for having produced widespread subduction-related potassic to ultrapotassic rocks (e.g., lamproites, leucites, and kamafugites; e.g., Avanzinelli et al., 2009; Conticelli et al., 2002; Lustrino & Wilson, 2007; Prelević et al., 2008). Previous studies have attributed the pronounced enrichments in incompatible elements and characteristic Sr-Nd isotopic compositions (radiogenic ⁸⁷Sr/⁸⁶Sr but unradiogenic ¹⁴³Nd/¹⁴⁴Nd) of the Mediterranean K-rich rocks to a strongly enriched lithospheric mantle source to which recycled crustal components have been added (Casalini et al., 2022; Lustrino et al., 2011; Prelević & Foley, 2007; Prelević et al., 2013; Y. Wang et al., 2021). However, whether or not the recycled crustal components are carbonate-rich is not well constrained, and the input flux of crustal carbon to the mantle sources is difficult to estimate using traditional geochemical proxies. Therefore, additional geochemical proxies are required to better constrain the source of carbon in the circum-Mediterranean lithospheric mantle and to provide a robust estimate for the input flux of carbon.

Magnesium and zinc isotopes are effective tools for tracing recycled carbonates in the mantle owing to the contrasting isotopic compositions of marine carbonates ($\delta^{26}\text{Mg} = -3.1 \pm 1.22\text{‰}$; $\delta^{66}\text{Zn} = 0.99 \pm 0.25\text{‰}$; e.g., S.-A. Liu et al., 2017; Pichat et al., 2003; Sweere et al., 2018; Teng, 2017) and the mantle ($\delta^{26}\text{Mg} = -0.25 \pm 0.04\text{‰}$ and $\delta^{66}\text{Zn} = 0.18 \pm 0.05\text{‰}$; S.-A. Liu et al., 2019; McCoy-West et al., 2018; Sossi et al., 2018; Teng, 2017; Z.-Z. Wang et al., 2017). Importantly, neither Mg nor Zn isotopes fractionate significantly during prograde metamorphic reactions (Inglis et al., 2017; S.-J. Wang et al., 2014) or magmatic processes (see reviews by Moynier et al., 2017; Teng, 2017). Therefore, Mg and Zn isotopic systematics of mantle-derived lavas can be used to identify the presence of recycled carbonates in their mantle sources. In this paper, we report the first Mg and Zn isotopic data for Cenozoic K-rich lavas around the circum-Mediterranean region (Spain, Italy, Serbia, Macedonia, and Turkey) and combine these results with Sr-Nd-Pb isotopes to elucidate the origin of carbonate metasomatism in the lithospheric mantle. In addition, we use Monte Carlo simulations of melting and mixing to estimate the input flux of recycled carbon into the mantle and compare this with the observed volcanic CO₂ outputs in this region. Our results indicate that subducted crustal carbon stored in the lithospheric mantle significantly contributed to the very high levels of subaerial volcanic CO₂ outgassing in the circum-Mediterranean region.

2. Geological Setting and Sample Description

Mantle-derived K-rich lavas occur in all major volcanic provinces along the Alpine–Himalayan orogenic belt (AHOB), which was formed by closure of the Tethyan Ocean in the Mesozoic (Prelević et al., 2013). They are volumetrically minor, but genetically important magmatic rocks as their geochemistry can be used as magmatic proxies to trace many lithospheric processes during orogenesis. The magmatic activity coincides with the major tectonic changes within the region from Cretaceous to Pleistocene (Conticelli et al., 2009), indicating that this episodic activation represents an integral aspect of the broader tectonic development (Lustrino et al., 2011). The circum-Mediterranean region (Figure 1) forms the western part of the AHOB and is associated with the pre-, syn- and post-collisional effects of anticlockwise convergence of the African-Arabian and Eurasian plates since the Permian-Mesozoic (Lustrino et al., 2011; Prelević & Foley, 2007). Seismic tomographic images reveal that distinct subducted slabs and slab fragments, which transferred crustal materials into the mantle, exist throughout the whole sub-Mediterranean region (Piromallo & Morelli, 2003). Subduction and subsequent post-collisional events resulted in the generation of widespread Cenozoic potassic-ultrapotassic lavas around the circum-Mediterranean region that are particularly suitable for investigation of metasomatic agents in the mantle (e.g., Ammannati et al., 2016; Prelević & Foley, 2007).

A total of 39 potassic-ultrapotassic volcanic rock samples from five areas (Figure 1) were selected for this study: Spain (Murcia-Almeria), Italy (Tuscany), Serbia (NW Vardar zone), Macedonia (Southern Vardar zone) and Turkey (Western Anatolia). These rocks were mainly emplaced in post-collisional extensional tectonic settings from Eocene to Pleistocene (Fritschle et al., 2013). They are mainly characterized by porphyritic textures with olivine (up to 10 vol%), phlogopite (up to 15 vol%) and clinopyroxene phenocrysts and clinopyroxene, sanidine, leucite, phlogopite, apatite, and oxides in the groundmass (Fritschle et al., 2013; Prelević et al., 2012).

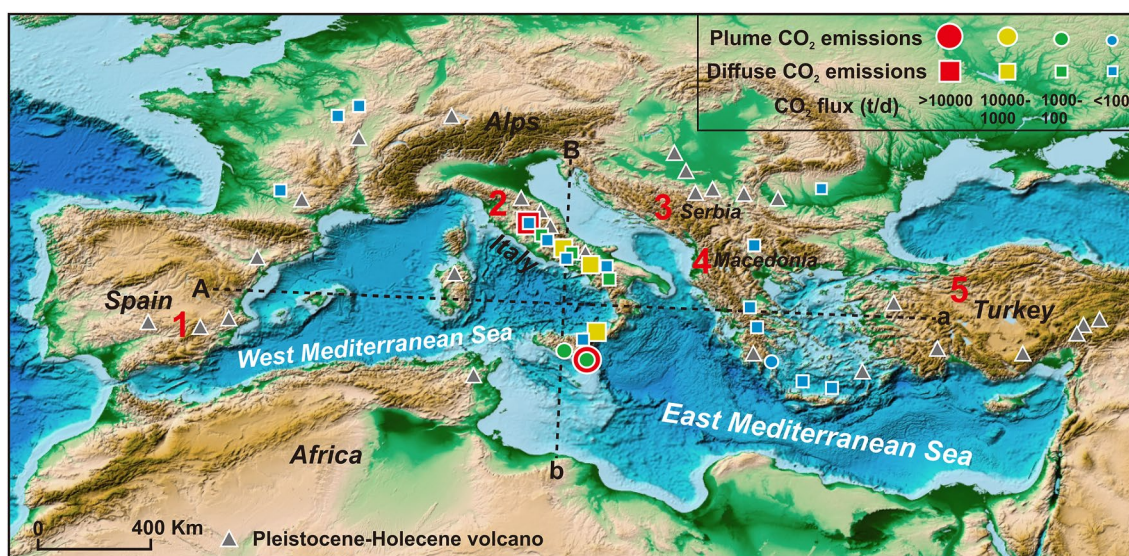


Figure 1. Digital topographic map of the circum-Mediterranean region (<http://www.ngdc.noaa.gov/mgg/global/global.html>). Red numbers from 1 to 5 denote localities of K-rich rocks analyzed in this study (Spain, Italy, Serbia, Macedonia, and Turkey in turn). The volcano locations and measured fluxes of CO₂ emissions by plume and diffusing are from Werner et al. (2019) and references therein.

Geochemically, they are extremely enriched in K₂O (K₂O/Na₂O = 0.1–10.4; K₂O + Na₂O = 4.4–13.2 wt%; Figures 2a and 2b; Table S4 in Supporting Information S1) and have broad ranges of SiO₂ (42.1–57.8 wt%) and MgO contents (1.6–16.7 wt%). The Serbian samples have lower K₂O/Na₂O (blue circles in Figure 2b), but this is due to post-magmatic analcimization of leucites which alters the original ultrapotassic compositions but does not affect most of the other trace elements or isotopic ratios in these samples (Prelević et al., 2004, 2005). The incompatible trace elements, especially the LILEs (e.g., Rb, K, Pb), are extremely enriched in these rocks in comparison with oceanic basalts (Figure 3). The Th peak (high Th/Yb) and Ba trough (low Ba/La) are two key chemical features of Mediterranean K-rich lavas (Figure 2d), indicating the involvement of sediment-derived melts instead of fluids in their mantle sources (Kirchenbaur & Münker, 2015).

Cretaceous flysch sediments from the Balkans are predominantly derived from the continental margin and are components of the overstep sequence above the ophiolitic mélangé. Their geochemistry has been proposed to represent the closest approximation of the average local crust, and therefore proved as a feasible representative for the recycled crustal end-member (e.g., Prelević et al., 2008; Sokol et al., 2020). In this study, we selected a flysch sediment sample from Prelević et al. (2008) (06FL03; Table S4 in Supporting Information S1) with high SiO₂ (62.3 wt%) and CaO (10.9 wt%) contents from the Vardar ophiolitic suture zone (Serbia). This flysch contains ~19.5 wt% of carbonates and has a relatively high Ca/Ti ratio (27.2) typical of carbonate-bearing sediments (carbonates >10 wt% and Ca/Ti > 10; Figure S1 in Supporting Information S1; Table S1 in Supporting Information S1; Qu et al., 2022), and can be regarded as the crustal component representative of carbonate-bearing silicate sediments (Prelević et al., 2005). All the above samples (*n* = 40) have been well studied in terms of petrology, chemistry and Sr-Nd-Pb isotopic compositions; detailed descriptions can be found in Prelević et al. (2012, 2015, 2008, 2005).

3. Analytical Methods

All chemical procedures for purification of Mg and Zn followed published methods (Gao et al., 2019; S.-A. Liu, Wang, Li, Huang, & Yang, 2016) and were carried out at the Isotope Geochemistry Laboratory of the China University of Geosciences, Beijing. For Mg isotope analysis, 2 mg whole-rock powder was weighed into 7 mL Teflon vials in a 1:3 (v/v) mixture of concentrated HF-HNO₃ and heated on a hot plate for >12 hr at 130°C–150°C. For Zn isotope analysis, 20 mg whole-rock powder was weighed and the sample digestion procedure was the same as that of Mg isotope analysis. After complete dissolution, 100 μl (containing ~20 μg Mg) or 1 ml (containing > 1 μg Zn) of each sample solution was loaded on 2 ml Bio-Rad cation exchange resin AG50W-X8 or 1 ml anion exchange resin AG1-X8 for Mg and Zn chromatographic purification, respectively.

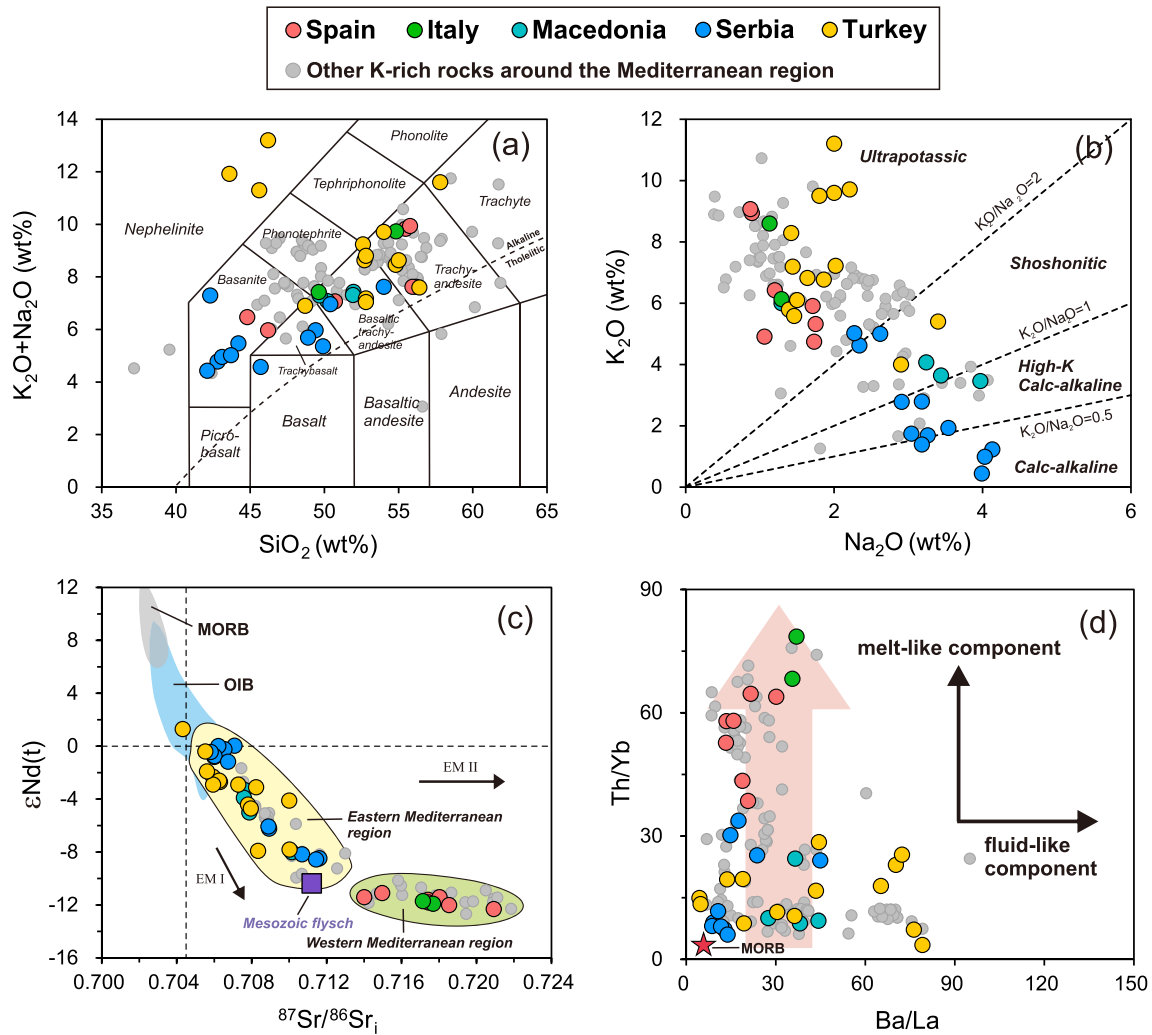


Figure 2. Geochemical characteristics of the circum-Mediterranean K-rich rocks. (a) Total alkali versus SiO₂ adapted from Le Bas et al. (1986). (b) K₂O versus Na₂O adapted from Foley (1992). (c) ⁸⁷Sr/⁸⁶Sr_i against εNd(t). The data for MORB and OIB are taken from the GEOROC database (<http://georoc.mpchmainz.gwdg.de/georoc/>). (d) Th/Yb versus Ba/La, illustrating the control of subduction components on the incompatible element budget of K-rich lavas (Kirchenbaur & Münker, 2015). Red star representing MORB is from Sun and McDonough (1989). Light gray circles represent other K-rich rocks around the Mediterranean region reported in Prelević et al. (2013). The chemical data are collected from Prelević et al. (2012, 2015, 2008, 2005) and listed in Table S4 in Supporting Information S1.

Magnesium was separated from matrix elements (K, Na, Ca, Fe, Al) by 1 N HNO₃, 8 N HCl, 0.4 N HCl and 0.5 N HNO₃ were used to achieve Zn purification. The same column procedures were repeated in order to assure the complete removal of matrix elements. After thorough drying, samples were dissolved in 1 ml 3% (m/m) HNO₃. The total recovery of Mg and Zn is more than 99%. Total procedural blank was 12 ng for Mg and 6 ng for Zn, which is very low in comparison with the amount of Mg (~20 μg) and Zn (>1 μg) in each loaded sample.

Analysis of Mg and Zn isotope ratios was carried out on a Thermo Scientific Neptune plus MC-ICP-MS. Purified samples dissolved in 3% (m/m) HNO₃ were introduced into the Ar plasma. Around 7.5 V signal of ²⁴Mg and 3.5 V signal of ⁶⁴Zn for a standard 10¹¹ Ω amplifier were obtained for a solution containing 400 ppb Mg and 200 ppb Zn, respectively. The sample-standard bracketing method was used for Mg isotopes to correct instrumental mass bias, while a Cu-doping technique following Maréchal et al. (1999) was utilized for mass bias correction of Zn isotopes. The Mg and Zn isotope ratios are reported in standard δ-notation in per mil relative to DSM-3 (Galy et al., 2003; Equation 1) and JMC 3-0749L (Maréchal et al., 1999; Equation 2), respectively:

$$\delta^{26,25}\text{Mg} (\text{‰}) = \left[\frac{(^{26,25}\text{Mg}/^{24}\text{Mg})_{\text{sample}}}{(^{26,25}\text{Mg}/^{24}\text{Mg})_{\text{DSM-3}}} - 1 \right] \times 1,000 \quad (1)$$

$$\delta^{68,66}\text{Zn} (\text{‰}) = \left[\frac{(^{68,66}\text{Zn}/^{64}\text{Zn})_{\text{sample}}}{(^{68,66}\text{Zn}/^{64}\text{Zn})_{\text{JMC 3-0749L}}} - 1 \right] \times 1,000 \quad (2)$$

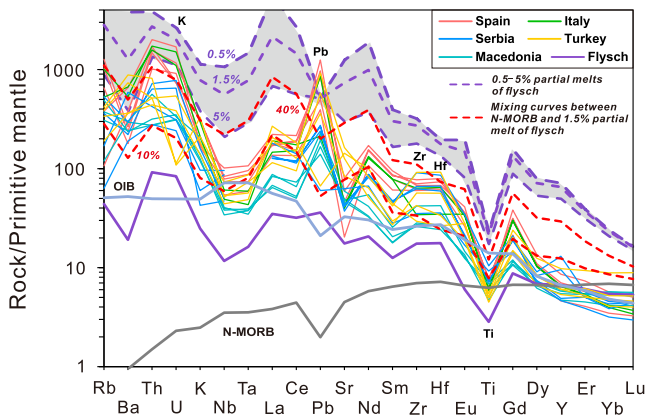


Figure 3. Primitive mantle-normalized trace element patterns of K-rich rocks in the circum-Mediterranean region. Data sources: Prelević et al. (2012, 2015, 2008, 2005). Data for the flysch sediment are from Prelević et al. (2008). The bulk partition coefficients for trace elements used in the flysch melting model are from Grassi et al. (2012), and the grey area represents the partial melting results of flysch ($F = 0.5\%$ – 5%). The end-members of the mixing curve are N-MORB (60%–90%) and the partial melt of flysch ($F = 1.5\%$; 10%–40%). The primitive mantle values are from McDonough and Sun (1995). Compositions of average OIB and N-MORB are from Sun and McDonough (1989).

The long-term external reproducibility (2sd) is $\pm 0.06\%$ for $\delta^{26}\text{Mg}$ (Gao et al., 2019) and $\pm 0.04\%$ for $\delta^{66}\text{Zn}$ (S.-A. Liu, Wang, Li, Huang, & Yang, 2016; Z.-Z. Wang et al., 2017) based on repeated analyses of synthetic solutions (GSB-Mg, IRMM 3702) and international rock standards (BHVO-2, BCR-2, etc.). The USGS reference materials BCR-2 ($\delta^{26}\text{Mg} = -0.23 \pm 0.06\%$; $\delta^{66}\text{Zn} = 0.27 \pm 0.02\%$) and BHVO-2 ($\delta^{26}\text{Mg} = -0.28 \pm 0.04\%$; $\delta^{66}\text{Zn} = 0.32 \pm 0.01\%$) analyzed in this study are consistent with literature data (Moynier et al., 2017; Sossi et al., 2015; Teng, 2017; Z.-Z. Wang et al., 2017). The uncertainties for $\delta^{26}\text{Mg}$ and $\delta^{66}\text{Zn}$ are given as 2sd throughout the text.

4. Results

The Mg and Zn isotopic data of the circum-Mediterranean K-rich lavas are reported in Table 1. These rocks show a wide range of $\delta^{26}\text{Mg}$ values from -0.61% to -0.21% ($n = 39$), which are similar to, or significantly lower than those of MORB and the mantle ($-0.25 \pm 0.04\%$; Teng, 2017; Figure 4). Zinc isotopic ratios display a narrow $\delta^{66}\text{Zn}$ range of 0.26% to 0.35% with an average of $0.31 \pm 0.04\%$ ($n = 39$), which is consistent with that of MORB ($0.27 \pm 0.06\%$; J. Huang et al., 2018; Z.-Z. Wang et al., 2017; Figure 4) within analytical uncertainty.

The carbonate-bearing Mesozoic flysch sediment (06FL03) has a $\delta^{26}\text{Mg}$ value of $-0.77 \pm 0.06\%$, distinctly lower than silicate sediments with $\delta^{26}\text{Mg}$ ranging from -0.52% to 0.92% (W.-Y. Li et al., 2010; S.-J. Wang et al., 2015),

but falls within the range of carbonate-bearing silicate sediments reported in the literature ($-0.51 \pm 0.68\%$; K.-J. Huang et al., 2013; Qu et al., 2022; S.-J. Wang et al., 2015; Wimpenny et al., 2014; Figure 4a). The $\delta^{66}\text{Zn}$ value of this sample ($0.27 \pm 0.05\%$) is much lower than that of marine carbonates ($0.99 \pm 0.25\%$; S.-A. Liu et al., 2017; Pichat et al., 2003; Sweere et al., 2018), but indistinguishable from that of MORB ($0.27 \pm 0.06\%$; J. Huang et al., 2018; Z.-Z. Wang et al., 2017) and carbonate-bearing silicate sediments ($0.26 \pm 0.08\%$; Qu et al., 2022; Figure 4b).

The most striking Mg and Zn isotopic characteristic of the circum-Mediterranean K-rich lavas is that most of them have $\delta^{26}\text{Mg}$ lower than mantle values but all samples have $\delta^{66}\text{Zn}$ values identical to those of MORB (Figure 4; Table 1). To our knowledge, such a signature has not yet been observed for other types of mantle-derived lavas. For instance, global oceanic island basalts (OIB) have mantle-like $\delta^{26}\text{Mg}$ (Teng, 2017) and similar or slightly higher $\delta^{66}\text{Zn}$ than those of MORB (Beunon et al., 2020). Some intraplate alkali basalts (e.g., Cenozoic basalts in East Asia) have lower $\delta^{26}\text{Mg}$ and higher $\delta^{66}\text{Zn}$ than these of the mantle (Figure 5; Table S5 in Supporting Information S1), which are labeled as “Mg-Zn isotopic coupling” and have been attributed to the recycling of sedimentary carbonates into the mantle sources (e.g., S.-G. Li et al., 2017; S.-A. Liu et al., 2022; S.-A. Liu, Wang, Li, Huang, & Yang, 2016). In contrast to “Mg-Zn isotopic coupling”, we consider this specific signature (low $\delta^{26}\text{Mg}$ but MORB-like $\delta^{66}\text{Zn}$) of the circum-Mediterranean K-rich lavas as “Mg-Zn isotopic decoupling” (Figure 5).

5. Discussion

In this part, we first discuss the origin of Mg-Zn isotopic decoupling in the circum-Mediterranean K-rich lavas, and then estimate the input flux of crustal carbon recycled into the circum-Mediterranean lithospheric mantle. Finally, we simulate the possible CO_2 output flux in this region and compare it with the observed subaerial volcanic CO_2 output flux.

5.1. The Origin of Mg-Zn Isotopic Decoupling in Circum-Mediterranean K-Rich Lavas

5.1.1. Effects of Low-Temperature and Magmatic Processes

Before linking the observed Mg and Zn isotopic signatures of the circum-Mediterranean K-rich lavas to mantle source heterogeneity, the potential influence of post-eruption low-temperature alteration, crustal contamination, magmatic differentiation, and kinetic isotope fractionation must be evaluated. Although some samples have relatively high loss on ignition (LOI) of 2.1–10.9 wt% (Table S4 in Supporting Information S1), their $\delta^{26}\text{Mg}$ and

Table 1

Mg-Zn Isotopic Compositions (‰) and Sr-Nd-Pb Isotopic Data for the Cenozoic K-Rich Rocks in the Circum-Mediterranean Region

Sample no.	Rock type	$\delta^{25}\text{Mg}$	2sd	$\delta^{26}\text{Mg}$	2sd	$\delta^{66}\text{Zn}$	2sd	$\delta^{68}\text{Zn}$	2sd	$^{87}\text{Sr}/^{86}\text{Sr}_i$	$\epsilon\text{Nd}(t)$	$^{206}\text{Pb}/^{204}\text{Pb}$	$^{207}\text{Pb}/^{204}\text{Pb}$	$^{208}\text{Pb}/^{204}\text{Pb}$
<i>Spain</i>														
03V16	Lamproite	-0.17	0.03	-0.33	0.02	0.30	0.02	0.59	0.06	0.72092	-12.3	18.78	15.69	38.98
03J09	Lamproite	-0.17	0.03	-0.34	0.05	0.31	0.01	0.62	0.04	0.71401	-11.4	18.8	15.72	39.09
03J10	Lamproite	-0.19	0.01	-0.37	0.01	0.30	0.02	0.59	0.01	0.71497	-11.1	18.84	15.78	39.3
03CX02	Lamproite	-0.14	0.06	-0.27	0.05	0.30	0.03	0.59	0.03	0.71741	-11.6	18.81	15.75	39.18
02CX05	Lamproite	-0.19	0.01	-0.37	0.02	0.31	0.02	0.61	0.03	0.71744	-11.8	18.81	15.74	39.16
03FC01	Lamproite	-0.17	0.04	-0.32	0.03	0.30	0.05	0.60	0.10	0.71803	-11.4	18.79	15.73	39.19
03FC02	Lamproite	-0.18	0.03	-0.34	0.03	0.28	0.04	0.55	0.03	0.71854	-12	18.76	15.7	39.06
<i>Italy</i>														
05RR02	Lamproite	-0.17	0.03	-0.32	0.05	0.35	0.06	0.70	0.06	0.71769	-11.9	18.67	15.71	39.08
05VDA03	Lamproite	-0.20	0.03	-0.37	0.06	0.32	0.03	0.63	0.09	0.71714	-11.7	18.63	15.7	38.99
<i>Serbia</i>														
Bo2-1	Lamproite	-0.12	0.02	-0.24	0.05	0.30	0.05	0.60	0.08	0.70893	-6.22	-	-	-
Bo2-2	Lamproite	-0.20	0.02	-0.39	0.04	0.34	0.03	0.67	0.03	0.70890	-6.07	-	-	-
BK01/3-1	Lamproite	-0.20	0.02	-0.39	0.04	0.31	0.04	0.61	0.02	0.71162	-8.47	18.73	15.68	38.88
BK01/3C	Lamproite	-0.18	0.03	-0.34	0.04	0.29	0.02	0.57	0.06	0.71069	-8.17	18.72	15.67	38.84
BK01/3A-2	Lamproite	-0.16	0.02	-0.32	0.03	0.31	0.01	0.63	0.02	0.71144	-8.55	-	-	-
KR01/1	Ugandite	-0.22	0.02	-0.44	0.04	0.28	0.02	0.55	0.07	0.706	-0.80	18.82	15.66	38.96
NV01/7	Ugandite	-0.16	0.04	-0.31	0.06	0.31	0.03	0.62	0.09	0.70709	0.04	18.75	15.66	38.83
NV01/4	Ugandite	-0.17	0.02	-0.32	0.02	0.29	0.06	0.57	0.03	0.70655	-0.21	18.75	15.67	38.87
NV01/6C	Lct-basanite	-0.11	0.02	-0.22	0.04	0.30	0.05	0.60	0.11	0.70622	0.02	18.76	15.68	38.9
TR01/2	Lct-basanite	-0.21	0.03	-0.41	0.06	0.30	0.02	0.58	0.06	0.70602	-0.74	18.78	15.65	38.88
TR01/1	Lct-basanite	-0.19	0.01	-0.36	0.04	0.32	0.04	0.62	0.04	0.70582	-0.43	18.74	15.64	38.82
DZI/2	Ankaratrite	-0.11	0.03	-0.22	0.04	0.33	0.04	0.66	0.05	0.70674	-1.17	18.76	15.68	38.92
<i>Macedonia</i>														
04CR02	Lamproite	-0.16	0.02	-0.32	0.03	0.31	0.03	0.62	0.05	0.70761	-3.3	18.84	15.72	39
04CR01	Lamproite	-0.18	0.04	-0.35	0.04	0.30	0.02	0.60	0.04	0.70759	-3.9	18.82	15.7	38.92
04SL01	Lamproite	-0.24	0.01	-0.46	0.02	0.35	0.03	0.69	0.02	0.70788	-5	18.81	15.69	38.93
03KK01	Lamproite	-0.12	0.04	-0.24	0.07	0.29	0.05	0.57	0.06	0.71015	-8	18.71	15.71	39.1
<i>Turkey</i>														
05KD012	Lamproite	-0.10	0.01	-0.21	0.01	0.34	0.04	0.68	0.13	0.71001	-4.1	18.91	15.71	38.97
06KD21	Lamproite	-0.13	0.00	-0.24	0.01	0.32	0.06	0.65	0.06	0.70781	-4.4	18.92	15.71	38.98
05GU01	Lamproite	-0.26	0.02	-0.55	0.01	0.27	0.05	0.54	0.14	0.70834	-7.9	18.94	15.75	39.25
05GU02	Lamproite	-0.21	0.02	-0.42	0.03	0.31	0.02	0.61	0.04	0.71002	-7.8	18.98	15.75	39.3
06AF03	Lamproite	-0.26	0.01	-0.51	0.02	0.29	0.08	0.58	0.09	0.70593	-2.3	18.84	15.7	38.88
06KZ01	Lamproite	-0.26	0.02	-0.51	0.03	0.29	0.04	0.57	0.06	0.70824	-3.1	19.07	15.7	38.97
05IL02	Lamproite	-0.12	0.01	-0.23	0.02	0.31	0.06	0.60	0.07	0.70729	-2.9	19.09	15.69	38.98
05BH05	Lamproite	-0.11	0.02	-0.21	0.02	0.30	0.05	0.60	0.09	0.70796	-4.7	18.98	15.7	38.97
31	Shoshonite	-0.12	0.01	-0.28	0.02	0.34	0.03	0.66	0.05	0.70553	-0.4	19.03	15.72	39.16
42	Tephriphonolite	-0.16	0.04	-0.35	0.04	0.31	0.04	0.62	0.00	0.70631	-2.7	18.68	15.7	38.71
29	Phonotephrite	-0.16	0.01	-0.32	0.02	0.34	0.03	0.66	0.04	0.70432	1.3	-	-	-
23/A	Tephriphonolite	-0.17	0.01	-0.33	0.02	0.32	0.04	0.62	0.10	0.70627	-2.6	18.69	15.7	38.72
19/A	Melilite-leucitite	-0.31	0.01	-0.61	0.01	0.31	0.01	0.61	0.03	0.70594	-2.9	18.85	15.72	38.92

Table 1
Continued

Sample no.	Rock type	$\delta^{25}\text{Mg}$	2sd	$\delta^{26}\text{Mg}$	2sd	$\delta^{66}\text{Zn}$	2sd	$\delta^{68}\text{Zn}$	2sd	$^{87}\text{Sr}/^{86}\text{Sr}_i$	$\epsilon\text{Nd}(t)$	$^{206}\text{Pb}/^{204}\text{Pb}$	$^{207}\text{Pb}/^{204}\text{Pb}$	$^{208}\text{Pb}/^{204}\text{Pb}$
1/A	Melilite-leucitite	-0.24	0.01	-0.46	0.02	0.26	0.04	0.51	0.03	0.70562	-1.9	19.1	15.74	39.24
<i>Flysch</i>														
06FL03		-0.39	0.03	-0.77	0.06	0.27	0.05	0.53	0.06	0.7112	-8.4	18.68	15.67	38.77
<i>Rock standards</i>														
BHVO-2		-0.14	0.02	-0.28	0.04	0.32	0.01	0.64	0.05					
BCR-2		-0.11	0.03	-0.23	0.06	0.27	0.02	0.53	0.03					

Note. Sr-Nd-Pb isotopic data are from Prelević et al. (2012, 2015, 2008, 2005). Sample localities, major and trace element data can be found in Table S4 in Supporting Information S1.

$\delta^{66}\text{Zn}$ values display no correlation with LOI ($R^2 = 0.00, 0.08$), indicating limited influence of post-magmatic alteration. The incompatible element (e.g., Sr, Nd, and Pb) concentrations of the K-rich rocks are about two times higher than those of continental crust (Prelević et al., 2008), so even considerable crustal contamination cannot explain their high incompatible element concentrations, which instead reflects mantle sources metasomatized by melts of subducted sediments. Moreover, in many cases, the high-MgO clinopyroxene phenocrysts in the K-rich rocks typically have $^{87}\text{Sr}/^{86}\text{Sr}$ ratios identical to their host rocks, implying isotopic equilibration between clinopyroxenes and K-rich lavas, which further excludes significant assimilation of crustal materials after clinopyroxene crystallization (Prelević et al., 2013). Fractional crystallization of olivine and/or Fe-Ti-Cr oxides would drive the residual melts to be enriched in ^{66}Zn with increasing SiO_2 because of the low $\delta^{66}\text{Zn}$ of olivine, while accumulation of olivine would deflect melts toward lower $\delta^{66}\text{Zn}$ with decreasing SiO_2 (H. Chen et al., 2013; Z.-Z. Wang et al., 2017; C. Yang et al., 2021). Fractional crystallization and accumulation of olivine or pyroxene

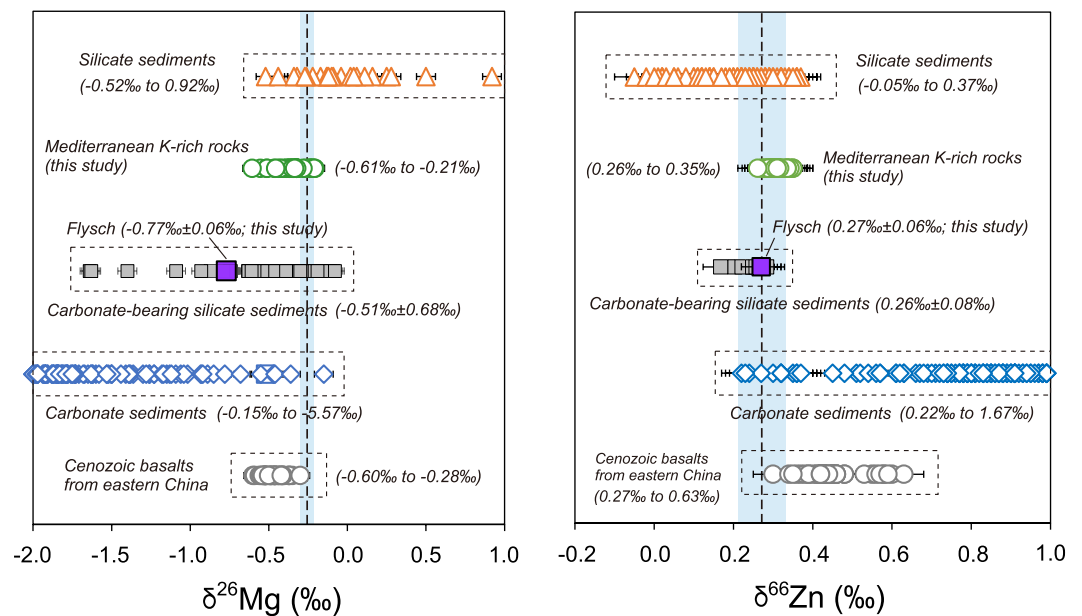


Figure 4. (a) $\delta^{26}\text{Mg}$ and (b) $\delta^{66}\text{Zn}$ of the circum-Mediterranean K-rich rocks, compared to those of silicate sediments, carbonate sediments, carbonate-bearing silicate sediments and <110 Ma intraplate alkali basalts in East Asia. The light blue bands represent the Mg-Zn isotopic data for MORB ($\delta^{26}\text{Mg} = -0.25 \pm 0.06\text{‰}$; Teng, 2017; $\delta^{66}\text{Zn} = 0.27 \pm 0.06\text{‰}$; J. Huang et al., 2018; Z.-Z. Wang et al., 2017). $\delta^{26}\text{Mg}$ data sources: silicate sediments (W.-Y. Li et al., 2010; S.-J. Wang et al., 2015), carbonate sediments (Teng, 2017 and references therein), carbonate-bearing silicate sediments (K.-J. Huang et al., 2013; Qu et al., 2022; S.-J. Wang et al., 2015; Wimpenny et al., 2014) and <110 Ma intraplate alkali basalts in East Asia (compiled in Table S5 in Supporting Information S1). $\delta^{66}\text{Zn}$ data sources: silicate sediments (Little et al., 2016; Maréchal et al., 2000; Vance et al., 2016), carbonate sediments (S.-A. Liu et al., 2017; Pichat et al., 2003; Sweere et al., 2018), carbonate-bearing silicate sediments (Qu et al., 2022) and <110 Ma intraplate alkali basalts in East Asia (Table S5 in Supporting Information S1).

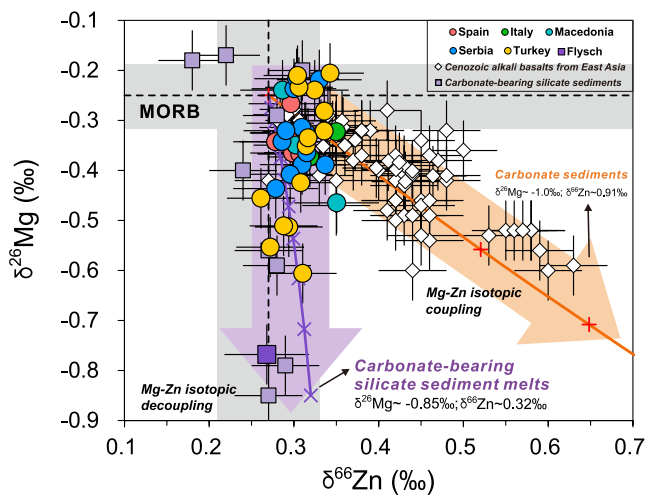


Figure 5. Plot of $\delta^{26}\text{Mg}$ versus $\delta^{66}\text{Zn}$ for the circum-Mediterranean K-rich rocks. The purple curve denotes binary mixing between MORB and carbonate-bearing silicate sediment-derived melts. The light purple squares are Mg-Zn isotopic data for carbonate-bearing silicate sediments in literature (Qu et al., 2022; Table S1 in Supporting Information S1). The $\delta^{66}\text{Zn}$ of carbonate-bearing silicate sediment melts is assumed to be 0.32‰. The orange curve denotes mixing between MORB and carbonate sediments (magnesite). The step sizes are 10%. The gray bands represent the Mg-Zn isotopic data for MORB ($\delta^{26}\text{Mg} = -0.25 \pm 0.06\text{‰}$; Teng, 2017; $\delta^{66}\text{Zn} = 0.27 \pm 0.06\text{‰}$; J. Huang et al., 2018; Z.-Z. Wang et al., 2017). The Mg-Zn isotopic data for magnesite and <110 Ma East Asia intraplate alkali basalts are from J. Huang et al. (2015), Jin et al. (2020), S.-G. Li et al. (2017), S.-A. Liu et al. (2016), Z.-Z. Wang and Liu (2021), Z.-Z. Wang et al. (2018), and W. Yang et al. (2012) (compiled in Table S5 in Supporting Information S1).

do not fractionate $\delta^{26}\text{Mg}$ of melts significantly (Teng et al., 2010). The lack of correlations between $\delta^{26}\text{Mg}$ or $\delta^{66}\text{Zn}$ and SiO_2 , MgO , and Cr contents ($R^2 = 0.01\text{--}0.05$; Figures 6a–6d) exclude any significant isotopic effects induced by magmatic differentiation. During the mantle partial melting, there is negligible Mg isotope fractionation (Teng, 2017) and only slight Zn isotope fractionation ($\delta^{66}\text{Zn}_{\text{melt-mantle}} \leq 0.08\text{‰}$; Sossi et al., 2018), suggesting that different degrees of partial melting is not a plausible cause for the decoupled Mg-Zn isotopic compositions of these K-rich rocks.

When basaltic melts ascend through the lithospheric mantle, potential temperature and chemical gradients exist between the melts and surrounding mantle peridotite, possibly inducing kinetic isotope fractionation. During thermal diffusion, lighter isotopes tend to concentrate in hot places (Richter et al., 2008) and thus in the ascending K-rich melts. This would result in lower values of both $\delta^{26}\text{Mg}$ and $\delta^{66}\text{Zn}$ in melts, which is inconsistent with the low $\delta^{26}\text{Mg}$ but unfractionated $\delta^{66}\text{Zn}$ of the K-rich lavas (Figure 5). During chemical diffusion, lighter isotopes diffuse faster than heavier ones along the chemical gradient (Richter et al., 2008). The K-rich melts have lower MgO contents (1.6–16.6 wt%) and higher Zn concentrations ($\sim 85.3 \mu\text{g/g}$) than those of the ambient mantle peridotites ($\text{MgO} \sim 38 \text{ wt\%}$ and $\text{Zn} \sim 55 \mu\text{g/g}$; Le Roux et al., 2010; McDonough & Sun, 1995). If chemical diffusion occurred, $\delta^{26}\text{Mg}$ and $\delta^{66}\text{Zn}$ of the melts would become appreciably lower and higher relative to those of MORB, respectively (S.-A. Liu & Li, 2019), which is inconsistent with the MORB-like $\delta^{66}\text{Zn}$ of the K-rich lavas (Figure 5). Hence, kinetic fractionation during thermal or chemical diffusion is unlikely to lead to the decoupled Mg-Zn isotopic compositions of these K-rich lavas.

5.1.2. The Key Role of Recycled Carbonate-Bearing Silicate Sediments in Mantle Sources

The Mediterranean K-rich rocks are characterized by strong enrichment in incompatible trace elements (especially LILEs; Figure 3), and high canonical trace element ratios like Pb/Ce (0.03–0.78), Cs/Rb (0.02–0.35) and Th/La (0.14–1.45) (Prelević et al., 2008; Tommasini et al., 2011; Y. Wang et al., 2021). They have highly radiogenic Sr and $^{207}\text{Pb}/^{204}\text{Pb}$ and unradiogenic Nd isotopic compositions compared to MORB and OIB ($^{87}\text{Sr}/^{86}\text{Sr} = 0.7043\text{--}0.7209$, $\epsilon\text{Nd} = -12.3\text{--}1.3$, and $^{207}\text{Pb}/^{204}\text{Pb} = 15.64\text{--}15.78$; Figure 7; Table 1). These features require one or more crustal components to have been recycled into their mantle sources (e.g., Conticelli & Peccerillo, 1992; Prelević et al., 2008, 2005). Here, we use Mg and Zn isotopes to decipher the type of recycled crustal components. Marine carbonate sediments typically have lighter Mg and heavier Zn isotopic compositions than those of the mantle (Figure 4). Thus, recycling of carbonates into the mantle via subduction will drive Mg and Zn isotopic compositions of the hybridized mantle toward lower and higher values, respectively, as widely observed in Cenozoic intraplate alkali basalts from East Asia (Figure 5; e.g., S.-G. Li et al., 2017; S.-A. Liu, Wang, Li, Huang, & Yang, 2016). The Mediterranean K-rich rocks have considerably lower $\delta^{26}\text{Mg}$ (-0.61‰ to -0.21‰) compared to MORB ($-0.25 \pm 0.04\text{‰}$; Teng, 2017), implying that the metasomatic agent most likely contains recycled carbonates given that marine carbonate is the only known crustal reservoir with extremely low $\delta^{26}\text{Mg}$. However, their MORB-like $\delta^{66}\text{Zn}$ (0.26‰ to 0.35‰) are inconsistent with the dominant role of recycled carbonates in the magma sources. The Mg-Zn isotopic decoupling, therefore, suggests a type of carbonate-related metasomatic agent that is distinct from marine carbonate sediments.

The low- $\delta^{26}\text{Mg}$ but MORB-like $\delta^{66}\text{Zn}$ signature of the Mediterranean K-rich rocks is in accordance with that of flysch sediment analyzed in this study ($\delta^{26}\text{Mg} = -0.77 \pm 0.06\text{‰}$, $\delta^{66}\text{Zn} = 0.27 \pm 0.05\text{‰}$; Figure 4), as well as carbonate-bearing silicate sediments from East Asia ($\delta^{26}\text{Mg} = -0.85$ to -0.17‰ , $\delta^{66}\text{Zn} = 0.18\text{--}0.31\text{‰}$) reported by Qu et al. (2022). To better understand the range and cause of Mg and Zn isotopic systematics of marine sediments that have the potential to be subducted, we compiled the available Mg-Zn isotopic data for carbonate sediments and silicate sediments (Figure 4). A large $\delta^{26}\text{Mg}$ difference of up to 6.49‰ exists between carbonate and silicate sediments (Figure 4a), indicating that carbonate components have a large impact on the $\delta^{26}\text{Mg}$ values of bulk sediments since they are the major carrier of light Mg isotopes in sediments. However, the $\delta^{66}\text{Zn}$ difference

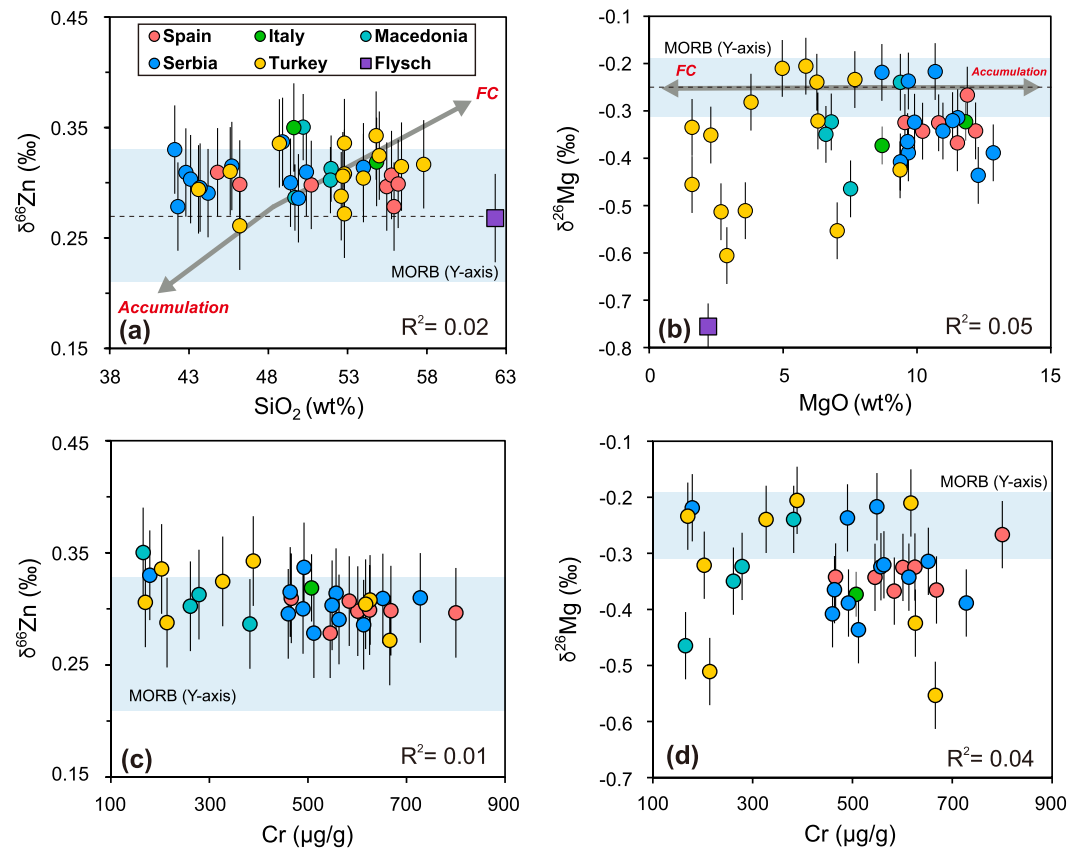


Figure 6. Plots of $\delta^{66}\text{Zn}$ versus SiO_2 (a) and $\delta^{26}\text{Mg}$ versus MgO (b). Gray arrows denote the magma evolution trend of the Kilauea Iki lavas, Hawaii (H. Chen et al., 2013; Teng et al., 2007). The light blue areas represent the Mg-Zn isotopic data for MORB ($\delta^{26}\text{Mg} = -0.25 \pm 0.06\text{‰}$; $\delta^{66}\text{Zn} = 0.27 \pm 0.06\text{‰}$; J. Huang et al., 2018; Teng, 2017; Z.-Z. Wang et al., 2017). Samples in this study do not fall on the Kilauea Iki trend, indicating negligible effect of fractional crystallization (FC) and accumulation. (c–d) Plots of $\delta^{26}\text{Mg}$ and $\delta^{66}\text{Zn}$ against Cr contents. The lack of correlations indicates that olivine and/or Fe-Ti-Cr oxides crystallization have negligible influence on Mg and Zn isotopic compositions of the circum-Mediterranean K-rich rocks. The chemical data are from Prelević et al. (2012, 2015, 2008, 2005).

between carbonate and silicate sediments (-0.15‰ to 1.72‰ ; Figure 4b) is much smaller than that of the $\delta^{26}\text{Mg}$ difference. Carbonate sediments also have lower Zn concentrations ($44 \pm 37 \mu\text{g/g}$; X. M. Liu et al., 2016 and references therein) than silicate sediments ($88 \pm 33 \mu\text{g/g}$; Plank, 2014 and references therein), although the former are generally similar to the Zn concentration of the mantle ($\sim 55 \mu\text{g/g}$; Le Roux et al., 2010). Consequently, carbonate components have only a limited impact on the $\delta^{66}\text{Zn}$ values of bulk sediments, which leads to almost identical Zn isotopic compositions for carbonate-bearing and carbonate-free silicate sediments (Figure 4b).

To further quantify the distinctive Mg-Zn isotopic compositions of the carbonate-bearing silicate sediments, we applied Monte Carlo models (see details in Table S2 in Supporting Information S1 and Data Set S1) in which carbonate components (e.g., CaCO_3) account for 5%–50% ($\text{CaO} = 2.8\text{--}28 \text{ wt\%}$) of bulk sediments. The results simulate the low $\delta^{26}\text{Mg}$ ($-1.03 \pm 1.05\text{‰}$; $n = 3,000$), MORB-like $\delta^{66}\text{Zn}$ ($0.28 \pm 0.13\text{‰}$), limited $^{206}\text{Pb}/^{204}\text{Pb}$ (18.74 ± 0.57) and high $^{207}\text{Pb}/^{204}\text{Pb}$ (15.69 ± 0.15) characteristics of carbonate-bearing silicate sediments successfully (Figure 7), implying that Mg-Zn isotopic decoupling with $\delta^{26}\text{Mg}$ lower than MORB but MORB-like $\delta^{66}\text{Zn}$ is a common feature of carbonate-bearing silicate sediments. Combined with the trace element patterns of the flysch sediments, namely positive anomalies of Rb, K, and Pb and negative anomalies of Nb, Ta, and Ti (Figure 3), we suggest that recycled carbonate-bearing silicate sediments are the most appropriate metasomatic agents operating in the source of the Mediterranean K-rich rocks. In addition, K-rich rocks from the western Mediterranean regions (Spain and Italy) possess significantly higher $^{87}\text{Sr}/^{86}\text{Sr}$ (Figures 7a and 7b) than the eastern ones (Serbia, Macedonia, and Turkey), suggesting that older upper continental crustal materials (UCC; e.g., Jurassic Tethyan sediments from Zermatt-Saas ophiolite with $^{87}\text{Sr}/^{86}\text{Sr}$ up to 0.727; Prelević et al., 2008) may have been involved in the western mantle sources.

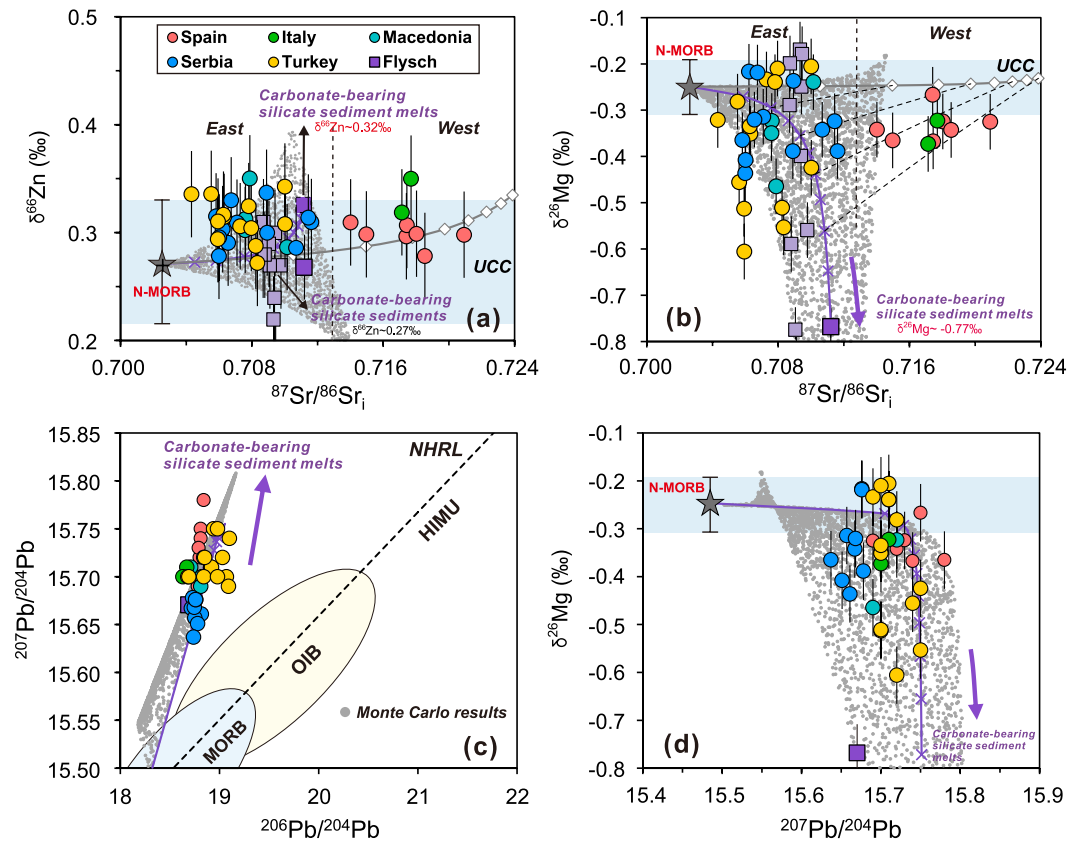


Figure 7. Plots of $^{87}\text{Sr}/^{86}\text{Sr}_i$ against $\delta^{66}\text{Zn}$ (a) and $\delta^{26}\text{Mg}$ (b). Plots of $^{207}\text{Pb}/^{204}\text{Pb}$ against $^{206}\text{Pb}/^{204}\text{Pb}$ (c) and $\delta^{26}\text{Mg}$ (d). The solid purple curve denotes mixing between N-MORB and carbonate-bearing silicate sediments (flysch). Another crustal component, upper continental crust (UCC), explains the extremely high $^{87}\text{Sr}/^{86}\text{Sr}$ of the western Mediterranean K-rich rocks. The gray dots represent the results of the Monte Carlo models, simulating the mixing between N-MORB and melts of carbonate-bearing silicate sediments. The light purple squares represent carbonate-bearing silicate sediment data in literature (Qu et al., 2022; Table S1 in Supporting Information S1). The light blue areas denote Mg and Zn isotopic compositions of MORB ($\delta^{26}\text{Mg} = -0.25 \pm 0.06\text{‰}$, Teng, 2017; $\delta^{66}\text{Zn} = 0.27 \pm 0.06\text{‰}$; J. Huang et al., 2018; Z.-Z. Wang et al., 2017). The Pb isotopic data for OIB and MORB are taken from the GEOROC database (<http://georoc.mpch-mainz.gwdg.de/georoc>). NHRL is the Northern Hemisphere Reference Line (Hart, 1984). East refers to Serbia, Macedonia, and Turkey; West to Spain and Italy. Details of the end-members, data sources and Monte Carlo models are listed in Table S2 in Supporting Information S1 and Data Set S1.

5.2. Widespread Carbonated Lithospheric Mantle Beneath the Circum-Mediterranean Region

In addition to samples in this study, other K-rich rocks from the central Mediterranean region (kamafugites and plagioclite) have also been demonstrated to have recycled carbonate-rich sediments in their mantle sources, which is clearly constrained by Sr and Nd isotopes and U/Th disequilibria (strong ^{238}U excesses; e.g., Avanzinelli et al., 2007; Conticelli et al., 2002; Conticelli & Peccerillo, 1992). Extremely low Ni (~1,000 ppm) and high Ca (up to 4,000 ppm) concentrations characterize highly forsteritic olivine phenocrysts of silica-undersaturated leucite-bearing ultrapotassic rocks in Italy, indicating strong mantle metasomatism by melts of carbonate-rich pelites that reacted with orthopyroxene to produce an olivine-rich mantle source (Ammannati et al., 2016; Conticelli et al., 2015, 2013). Among the K-rich rocks analyzed in this study, leucite-free samples (lamproite) also display Mg-Zn isotopic decoupling ($\delta^{26}\text{Mg} = -0.55$ to -0.21‰ , $\delta^{66}\text{Zn} = 0.27$ – 0.35‰ ; $n = 27$; Table 1), which is indistinguishable from that of leucite-bearing rocks (ugandite, leucite-basanite, ankaratrite and melilite-leucite; $\delta^{26}\text{Mg} = -0.61$ to -0.22‰ , $\delta^{66}\text{Zn} = 0.26$ – 0.33‰ ; $n = 9$; Table 1). Low $\delta^{26}\text{Mg}$ values have also been discovered in lamproites from the Leucite Hills ($\delta^{26}\text{Mg} = -0.43$ to -0.37‰ ; Sun et al., 2021) and high-MgO lamproites from Eastern China ($\delta^{26}\text{Mg} = -0.59$ to -0.35‰ ; Z. X. Wang et al., 2022). Therefore, we suggest that the mantle sources of these circum-Mediterranean K-rich rocks are widely metasomatized by carbonate-bearing silicate sediments.

It has previously been suggested that the generation of strongly potassic, mantle-derived melts requires the presence of phlogopite in their mantle sources (Foley, 1992). Recent studies investigating the reaction between continental sediments and depleted peridotite and a mixture of glimmerite and harzburgite demonstrate that potassic to ultrapotassic melts can be formed at 1–3 GPa and 1000°C–1300°C, corresponding to shallow lithospheric mantle thermobaric conditions (Förster et al., 2017; Y. Wang, Foley, & Prelević, 2017). Moreover, high-Mg[#] ([atomic Mg/(Mg + Fe)]; up to 0.95) olivine phenocrysts with high-Cr[#] spinel inclusions ([atomic Cr/(Cr + Al)]; around 0.95) in Mediterranean K-rich rocks suggest an ultra-depleted lithospheric mantle source, most likely derived from an island-arc oceanic lithosphere accreted during Alpine collisional processes (Prelević & Foley, 2007). Thus, the source region of the circum-Mediterranean K-rich rocks is probably located at lithospheric mantle depths at which carbonate-bearing silicate sediments carried by subducted slabs may be recycled, probably as imbricated blocks (Y. Wang et al., 2021), where they contribute to magma sources. These K-rich rocks plot along the strong curvature of the hyperbolic arrays (Sr-Nd-Pb-Mg isotopes; Figures 2c and 7b–7d), indicating mixing of melts of contrasting compositions in the mantle instead of mixing of source rocks. The eastern Mediterranean samples resulted from binary mixing between carbonate-bearing silicate sediment and MORB-like melts that were most likely derived from the depleted lithospheric mantle upon heating or decompression, while three end-member mixing including melts of carbonate-bearing silicate sediment, the depleted lithospheric mantle and UCC generated the western Mediterranean samples (Figure 7). Förster et al. (2019) carried out an experiment investigating the role of sediment and peridotite-derived melts in the formation of potassic magmatism. The experimental results show that the partial melts of sediments and dunite form a reaction zone in which the infiltrating melts display major and trace element compositions similar to those of the circum-Mediterranean K-rich lavas (Prelević et al., 2008), implying that mixing between mantle-derived melts (e.g., MORB-like melts) and melts of sediments can generate K-rich lavas. Geophysical tomographic data further support this interpretation: a low *S* wave velocity (*V_s*) layer at a depth of approximately 60–130 km is present beneath the western Mediterranean (Panza, Peccerillo, et al., 2007; Panza, Raykova, et al., 2007) and is attributed to carbon-rich melts originating from melting of continent-derived sediments and/or the subducted African continental crust (Frezzotti et al., 2009). Similar tomographic images are also found for the eastern Mediterranean domain where a high *V_s* layer indicating a subducting slab is located at 100–200 km and a low *V_s* layer exists at 50–100 km above the slab (Elgabry et al., 2013).

Geodynamically, the circum-Mediterranean region has experienced long-lasting convergence resulting from subduction of the major Tethyan oceanic slabs. The metasomatic agents (carbonate-bearing silicate sediments) responsible for these K-rich lavas are derived from the subducting slab, and are situated within the lithospheric mantle typically forming veins and dykes dominantly composed of hydrous minerals (e.g., Conceição & Green, 2004; Conticelli & Peccerillo, 1992). Moreover, the closure of small oceanic basins may be facilitated by intra-oceanic subduction which was probably common during Mesozoic Mediterranean Tethyan geodynamics (Robertson, 2002). Supra-subduction-related volcanism would leave behind a strongly depleted mantle area which should be more buoyant relative to surrounding asthenosphere, and the depleted oceanic lithospheric mantle was accreted to the continent during Alpine collisional processes (Prelević & Foley, 2007). The mixing between low-degree melts of these metasomatic veins and melts derived from the depleted lithospheric mantle results in the most extreme ultrapotassic lavas like lamproites and kamafugites, whereas with larger extents of melting, melt-mantle interaction and assimilation of the material from the ambient depleted mantle will result in more voluminous, but less alkaline magmatism (shoshonitic to calc-alkaline series), which is widespread in several major volcanic provinces in the circum-Mediterranean region such as Italy, Spain, Turkey (e.g., Conticelli et al., 2009; Prelević et al., 2012, 2008; Tappe et al., 2006). Therefore, the wide distribution of K-rich lavas (Figure 1) may be an indication of the large-scale presence of carbonated lithospheric mantle beneath the circum-Mediterranean region.

5.3. Estimation of Carbon Input Flux Into the Lithospheric Mantle

To quantify the amount of carbonate-bearing silicate sediment in the sources of the circum-Mediterranean K-rich lavas, we develop a binary mixing simulation between primitive mantle-derived melts (represented by MORB) and melts derived from partial melting of carbonate-bearing sediments. Different degrees of partial melting ($F = 0.5\%–5\%$; Figure 3) are assumed for the carbonate-bearing sediments, following Equation 3 below (Wilson, 1989):

$$C_{X\text{-sediment melts}} = C_{X\text{-sediments}} / [(1 - F) \times D_X + F] \quad (3)$$

where X is Mg, Zn, Sr or Pb, $C_{X\text{-sediments}}$ are the element concentrations for flysch sediment listed in Table 1, and D_X is the bulk partition coefficient from Grassi et al. (2012). The binary mixing simulation is calculated with Equations 4 and 5 (Faure & Mensing, 2004):

$$C_X = C_{X\text{-sediment melts}} \times \lambda + C_M \times (1 - \lambda) \quad (4)$$

$$R_X = R_{X\text{-sediment melts}} \times \lambda \times (C_{X\text{-sediment melts}}/C_X) + R_M \times (1 - \lambda) \times (C_M/C_X) \quad (5)$$

where C_X and R_X are element concentrations and isotopic ratios ($\delta^{26}\text{Mg}$, $\delta^{66}\text{Zn}$, $^{87}\text{Sr}/^{86}\text{Sr}$, $^{206}\text{Pb}/^{204}\text{Pb}$, and $^{207}\text{Pb}/^{204}\text{Pb}$) after mixing, respectively, λ is the proportion of melt derived from carbonate-bearing silicate sediments (flysch), C_M and R_M are element concentrations and isotopic ratios of MORB (data listed in Table S2 in Supporting Information S1), and $R_{X\text{-sediment melts}}$ are Mg, Zn, Sr, or Pb isotopic ratios of flysch sediments (Table 1). The $\delta^{66}\text{Zn}$ of flysch melts is assumed to be 0.32‰.

The results of binary mixing models based on Zn-Mg-Sr-Pb isotopes (Figures 6 and 7) and trace elements (Figure 3) indicate that about 10%–40% (λ) melts of carbonate-bearing silicate sediment are required to generate these K-rich rocks. To acquire the input flux of recycled carbon (M_{input}), we use a Monte Carlo model as follows:

$$M_{\text{input}} (\text{Mt/yr}) = \frac{Aa \times Bb \times x \times y \times \lambda \times W_c \times W_{cc} \times \rho_c}{z} \quad (6)$$

where Aa (2,300 km) and Bb (900 km) represent the length and width of the region (Figure 1), x (1–50 km; Panza, Peccerillo, et al., 2007; Panza, Raykova, et al., 2007) is the thickness of the metasomatized lithospheric mantle, y (0%–50%) is the percentage by area of the mantle that has been metasomatized, λ (10%–40%) is the mass fraction of carbonate-bearing silicate sediment melts calculated above, W_c (5%–50%) is the proportion of carbonates in the carbonate-bearing silicate sediments, W_{cc} (13%) is the mass fraction of C in carbonates (assumed to be dolomite), ρ_c (2.4×10^{15} g/km³) is the density of carbonate melts in the upper mantle (Ritter et al., 2020), and z (35 Ma) is the initial eruption age of the K-rich magmas (Prelević et al., 2013). The x , y , λ , and W_c are taken randomly within the given reasonable range by the Monte Carlo model (see Data Set S2) and an average M_{input} value of about 8.1 Mt/yr is obtained (Figure S2 in Supporting Information S1). A previous study speculated that there might be an unusually high carbon input flux into the Tethyan lithosphere (Plank & Manning, 2019), and our results suggest that a significant flux of carbon (~ 8.1 Mt/yr) from carbonate-bearing sediments has been recycled and stored in the lithospheric mantle beneath the circum-Mediterranean region, accounting for $\sim 14\%$ of the global carbon input flux from subducting sediments (57–60 Mt/yr; Clift, 2017; Dutkiewicz et al., 2018).

5.4. Implications for Subaerial Volcanic CO₂ Outgassing

Globally, volcanic CO₂ emissions are commonly sourced from the mantle, the downgoing slabs, and/or the overlying crust above subduction zones (Werner et al., 2019 and references therein). Previous studies combined $\delta^{13}\text{C}$ with $^3\text{He}/^4\text{He}$ data to define the origin of arc volcanic CO₂. Carbon isotopic compositions show a striking difference between mantle ($-6.0 \pm 2.0\%$) and surface carbonate ($\sim 0\%$) (Mason et al., 2017 and references therein). Mantle-derived CO₂ commonly has high $^3\text{He}/^4\text{He}$ (e.g., MORB = 8 ± 1 Ra; Graham, 2002), whereas low $^3\text{He}/^4\text{He}$ ratios are indicative of a source from the overlying crust. The $\delta^{13}\text{C}$ - $^3\text{He}/^4\text{He}$ data of global arc gases reveal that few samples fall in the depleted mantle range, indicating that the mantle carbon is not the major source of volcanic CO₂ (Werner et al., 2019). In the circum-Mediterranean region, studies of volcanic CO₂ have been mostly carried out in Italy, where about 43% of the inorganic carbon in degassing CO₂ is derived from deep sources with heavy $\delta^{13}\text{C}$ (-3 to 1%), implying mantle sources metasomatized by crustal components (Chiodini et al., 2000, 2004). Compiled gas data with high $^3\text{He}/^4\text{He}$ ratios (R/Ra up to 4.5; Frezzotti et al., 2009; Minissale, 2004) also imply metasomatized mantle sources rather than crustal assimilation. Therefore, subducted carbon is the main control of the isotopic composition and the amount of CO₂ at arc volcanoes. Combined with the carbon input flux estimated above for the circum-Mediterranean region (~ 8.1 Mt/yr), subducted carbon recycled into the lithospheric mantle should have a significant impact on volcanic CO₂ emissions.

To form a possible genetic connection between carbon input and output in the study area, we evaluate the flux of subaerial volcanic CO₂ emissions (M_{CO_2}) from the circum-Mediterranean lithospheric mantle using Equation 7:

$$M_{\text{CO}_2} (\text{Mt/yr}) = M_{\text{input}} \times \varepsilon \times 44/12 \quad (7)$$

where ϵ is the rational recycling efficiency of subducted carbon to the atmosphere through subaerial volcanoes (60%–90%; Oppenheimer et al., 2014; Plank & Manning, 2019). ϵ is taken randomly within the given range by the Monte Carlo model (see Data Set S2). The calculated average flux of M_{CO_2} around the circum-Mediterranean region is estimated to be about 22.4 Mt/yr (Figure S2 in Supporting Information S1), which fits the observed value well (20.1 ± 13.4 Mt/yr; 1sd; Table S3 in Supporting Information S1; Werner et al., 2019).

In the Mesozoic era, due to the warm climate and high sea levels flooding large expanses of the continents, there were large quantities of sedimentary carbonates when the seafloor of the shallow Tethyan ocean started to subduct (Lee et al., 2012; Plank & Manning, 2019). It is therefore reasonable to infer that abundant carbon was subducted at this time and stored in the lithospheric mantle (8.1 Mt/yr C), later to become the main source of the large subaerial volcanic CO₂ emissions (6.1 Mt/yr C) in the circum-Mediterranean region. Previous studies have suggested that carbonate sediments account for a large part of the subducting flux of carbon (>70%; Kelemen & Manning, 2015; Plank & Manning, 2019), and CO₂-He systematics for arcs worldwide indicate that carbonate sediments contribute about 50%–80% CO₂ to volcanic outputs (Oppenheimer et al., 2014). Therefore, subducted carbon and its storage in the lithospheric mantle (Bragagni et al., 2022; Foley & Fischer, 2017) is likely to be an important source for global subaerial volcanic CO₂ emissions, as reflected in the circum-Mediterranean region that accounts for about 20% of the global total.

6. Conclusions

We report the first Mg and Zn isotopic data for the well-studied Cenozoic K-rich lavas around the circum-Mediterranean region (Spain, Italy, Serbia, Macedonia, and Turkey) to investigate the nature of recycled crustal components in their mantle sources, with special emphasis on understanding the source of the high levels of volcanic CO₂ emissions in this area. The K-rich lavas display variable and systematically lower $\delta^{26}\text{Mg}$ than that of the mantle, but have $\delta^{66}\text{Zn}$ values consistent with those of primitive mantle-derived melts. The distinctive Mg-Zn isotopic composition of the circum-Mediterranean K-rich lavas is therefore “decoupled” and can be best explained as a result of source metasomatism by carbonate-bearing silicate sediments. Together with Mg-Zn-Sr-Pb isotopic data, binary mixing simulations suggest that about 10%–40% of carbonate-bearing silicate sediments have been recycled to the mantle sources of Mediterranean K-rich lavas. Considering that these K-rich lavas were derived from lithospheric mantle depths, we infer that a large amount of recycled carbon carried by subducted slabs is stored in the lithospheric mantle beneath this region. The carbon input flux from subducted slabs in the circum-Mediterranean region is estimated to be 8.1 Mt/yr. The subaerial volcanic CO₂ output flux is estimated to be 22.4 Mt/yr, which is in accordance with the observed value of 20.1 Mt/yr. Therefore, the recycled carbon stored in lithospheric mantle is likely a critical source for the enormous subaerial volcanic CO₂ emissions around the circum-Mediterranean region.

The combination of Mg and Zn isotopes proves useful to distinguish between the recycling of carbonate-bearing silicate sediments and carbonate-rich sediments, which are characterized by the diverging trends in Figure 5. This may in turn indicate the tectonic environment in which subduction occurred, with collages of small plates and continental blocks such as in the Mediterranean producing Mg-Zn isotopic decoupling. In contrast, the isotopic coupling may indicate the involvement of carbonate-rich sediments, which may be characteristic for larger-scale convergent margins (C. Chen et al., 2021).

Data Availability Statement

Supporting Information includes Figures S1–S2, Tables S1–S5 in Supporting Information S1 and Data Sets S1–S2. Mg and Zn isotopic data for the Cenozoic K-rich rocks in the circum-Mediterranean region and all supporting information related to this article are available at <https://doi.org/10.5281/zenodo.7420592>. Cite as: Shu et al. (2022).

References

- Ammannati, E., Jacob, D. E., Avanzinelli, R., Foley, S. F., & Conticelli, S. (2016). Low Ni olivine in silica-undersaturated ultrapotassic igneous rocks as evidence for carbonate metasomatism in the mantle. *Earth and Planetary Science Letters*, 444, 64–74. <https://doi.org/10.1016/j.epsl.2016.03.039>
- Avanzinelli, R., Casalini, M., Elliott, T., & Conticelli, S. (2018). Carbon fluxes from subducted carbonates revealed by uranium excess at Mount Vesuvius, Italy. *Geology*, 46(3), 259–262. <https://doi.org/10.1130/g39766.1>
- Avanzinelli, R., Elliott, T., Tommasini, S., & Conticelli, S. (2007). Constraints on the genesis of potassium-rich Italian volcanic rocks from U/Th disequilibrium. *Journal of Petrology*, 49(2), 195–223. <https://doi.org/10.1093/ptrology/egm076>

Acknowledgments

The authors are greatly grateful to editor Mark Dekkers and associate editor Philip Janney for their efficient handling and constructive comments. The authors also thank the anonymous reviewer for the careful comments and suggestions that helped to improve the manuscript. The authors thank Hai-Bo Ma and Meng-Lun Li for their help in the lab. This work was financially supported by the National Natural Science Foundation of China (41730214) and the National Key R&D Program of China (2019YFA0708400). D. P. and V. C. were supported by the Science Fund of the Republic of Serbia through project RECON TETHYS (7744807). V. C. was supported by the Serbian Academy of Sciences, Projects F9 and F17.

- Avanzinelli, R., Lustrino, M., Mattei, M., Melluso, L., & Conticelli, S. (2009). Potassic and ultrapotassic magmatism in the circum-Tyrrhenian region: Significance of carbonated pelitic versus pelitic sediment recycling at destructive plate margins. *Lithos*, *113*(1–2), 213–227. <https://doi.org/10.1016/j.lithos.2009.03.029>
- Beunon, H., Mattielli, N., Doucet, L. S., Moine, B., & Debret, B. (2020). Mantle heterogeneity through Zn systematics in oceanic basalts: Evidence for a deep carbon cycling. *Earth-Science Reviews*, *205*, 103174. <https://doi.org/10.1016/j.earscirev.2020.103174>
- Bragagni, A., Mastroianni, F., Münker, C., Conticelli, S., & Avanzinelli, R. (2022). A carbon-rich lithospheric mantle as a source for the large CO₂ emissions of Etna volcano (Italy). *Geology*, *50*(4), 486–490. <https://doi.org/10.1130/g49510.1>
- Casalini, M., Avanzinelli, R., Tommasini, S., Natali, C., Bianchini, G., Prelević, D., et al. (2022). Petrogenesis of Mediterranean lamproites and associated rocks: The role of overprinted metasomatic events in the post-collisional lithospheric upper mantle. *Geological Society, London, Special Publications*, *513*(1), 271–296. <https://doi.org/10.1144/sp513-2021-36>
- Chen, C., Forster, M. W., Foley, S. F., & Liu, Y. (2021). Massive carbon storage in convergent margins initiated by subduction of limestone. *Nature Communications*, *12*(1), 4463. <https://doi.org/10.1038/s41467-021-24750-0>
- Chen, H., Savage, P. S., Teng, F.-Z., Helz, R. T., & Moynier, F. (2013). Zinc isotope fractionation during magmatic differentiation and the isotopic composition of the bulk Earth. *Earth and Planetary Science Letters*, *369–370*, 34–42. <https://doi.org/10.1016/j.epsl.2013.02.037>
- Chiodini, G., Cardellini, C., Amato, A., Boschi, E., Caliro, S., Frondini, F., & Ventura, G. (2004). Carbon dioxide Earth degassing and seismogenesis in central and southern Italy. *Geophysical Research Letters*, *31*(7). <https://doi.org/10.1029/2004gl019480>
- Chiodini, G., Frondini, F., Cardellini, C., Parello, F., & Peruzzi, L. (2000). Rate of diffuse carbon dioxide Earth degassing estimated from carbon balance of regional aquifers: The case of central Apennine, Italy. *Journal of Geophysical Research: Solid Earth*, *105*(B4), 8423–8434. <https://doi.org/10.1029/1999jb900355>
- Clift, P. D. (2017). A revised budget for Cenozoic sedimentary carbon subduction. *Reviews of Geophysics*, *55*(1), 97–125. <https://doi.org/10.1002/2016rg000531>
- Conceição, R., & Green, D. (2004). Derivation of potassic (shoshonitic) magmas by decompression melting of phlogopite + pargasite lherzolite. *Lithos*, *72*(3–4), 209–229. <https://doi.org/10.1016/j.lithos.2003.09.003>
- Conticelli, S., Avanzinelli, R., Ammannati, E., & Casalini, M. (2015). The role of carbon from recycled sediments in the origin of ultrapotassic igneous rocks in the Central Mediterranean. *Lithos*, *232*, 174–196. <https://doi.org/10.1016/j.lithos.2015.07.002>
- Conticelli, S., Avanzinelli, R., Poli, G., Braschi, E., & Giordano, G. (2013). Shift from lamproite-like to leucititic rocks: Sr-Nd-Pb isotope data from the Monte Cimino volcanic complex versus the Vico stratovolcano, central Italy. *Chemical Geology*, *353*, 246–266. <https://doi.org/10.1016/j.chemgeo.2012.10.018>
- Conticelli, S., D'Antonio, M., Pinarelli, L., & Civetta, L. (2002). Source contamination and mantle heterogeneity in the genesis of Italian potassic and ultrapotassic volcanic rocks: Sr-Nd-Pb isotope data from Roman Province and Southern Tuscany. *Mineralogy and Petrology*, *74*(2), 189–222. <https://doi.org/10.1007/s007100200004>
- Conticelli, S., Guarneri, L., Farinelli, A., Mattei, M., Avanzinelli, R., Bianchini, G., et al. (2009). Trace elements and Sr-Nd-Pb isotopes of K-rich, shoshonitic, and calc-alkaline magmatism of the western Mediterranean region: Genesis of ultrapotassic to calc-alkaline magmatic associations in a post-collisional geodynamic setting. *Lithos*, *107*(1–2), 68–92. <https://doi.org/10.1016/j.lithos.2008.07.016>
- Conticelli, S., & Peccerillo, A. (1992). Petrology and geochemistry of potassic and ultrapotassic volcanism in central Italy: Petrogenesis and inferences on the evolution of the mantle sources. *Lithos*, *28*(3–6), 221–240. [https://doi.org/10.1016/0024-4937\(92\)90008-M](https://doi.org/10.1016/0024-4937(92)90008-M)
- Dasgupta, R., & Hirschmann, M. M. (2010). The deep carbon cycle and melting in Earth's interior. *Earth and Planetary Science Letters*, *298*(1–2), 1–13. <https://doi.org/10.1016/j.epsl.2010.06.039>
- Dutkiewicz, A., Müller, R. D., Cannon, J., Vaughan, S., & Zahirovic, S. (2018). Sequestration and subduction of deep-sea carbonate in the global ocean since the Early Cretaceous. *Geology*, *47*(1), 91–94. <https://doi.org/10.1130/g45424.1>
- Elgabry, M. N., Panza, G. F., Badawy, A. A., & Ibrahim, M. K. (2013). Imaging a relic of complex tectonics: The lithosphere-asthenosphere structure in the eastern Mediterranean. *Terra Nova*, *25*(2), 102–109. <https://doi.org/10.1111/ter.12011>
- Faure, G., & Mensing, T. M. (2004). *Isotopes: Principles and applications* (3rd ed.). John Wiley.
- Foley, S. F. (1992). Petrological characterization of the source components of potassic magmas: Geochemical and experimental constraints. *Lithos*, *28*(3–6), 187–204. [https://doi.org/10.1016/0024-4937\(92\)90006-k](https://doi.org/10.1016/0024-4937(92)90006-k)
- Foley, S. F., & Fischer, T. P. (2017). An essential role for continental rifts and lithosphere in the deep carbon cycle. *Nature Geoscience*, *10*(12), 897–902. <https://doi.org/10.1038/s41561-017-0002-7>
- Förster, M. W., Prelević, D., Buhre, S., Mertz-Kraus, R., & Foley, S. F. (2019). An experimental study of the role of partial melts of sediments versus mantle melts in the sources of potassic magmatism. *Journal of Asian Earth Sciences*, *177*, 76–88. <https://doi.org/10.1016/j.jseas.2019.03.014>
- Förster, M. W., Prelević, D., Schmück, H. R., Buhre, S., Veter, M., Mertz-Kraus, R., et al. (2017). Melting and dynamic metasomatism of mixed harzburgite + glimmerite mantle source: Implications for the genesis of orogenic potassic magmas. *Chemical Geology*, *455*, 182–191. <https://doi.org/10.1016/j.chemgeo.2016.08.037>
- Frezzotti, M. L., Peccerillo, A., & Panza, G. (2009). Carbonate metasomatism and CO₂ lithosphere-asthenosphere degassing beneath the western Mediterranean: An integrated model arising from petrological and geophysical data. *Chemical Geology*, *262*(1–2), 108–120. <https://doi.org/10.1016/j.chemgeo.2009.02.015>
- Fritschle, T., Prelević, D., Foley, S. F., & Jacob, D. E. (2013). Petrological characterization of the mantle source of Mediterranean lamproites: Indications from major and trace elements of phlogopite. *Chemical Geology*, *353*, 267–279. <https://doi.org/10.1016/j.chemgeo.2012.09.006>
- Galy, A., Yoffe, O., Janney, P. E., Williams, R. W., Cloquet, C., Alard, O., et al. (2003). Magnesium isotope heterogeneity of the isotopic standard SRM980 and new reference materials for magnesium-isotope-ratio measurements. *Journal of Analytical Atomic Spectrometry*, *18*(11), 1352. <https://doi.org/10.1039/b309273a>
- Gao, T., Ke, S., Li, R., Meng, X. n., He, Y., Liu, C., et al. (2019). High-precision magnesium isotope analysis of geological and environmental reference materials by multiple-collector inductively coupled plasma mass spectrometry. *Rapid Communications in Mass Spectrometry*, *33*(8), 767–777. <https://doi.org/10.1002/rcm.8376>
- Graham, D. W. (2002). Noble gas isotope geochemistry of mid-ocean ridge and ocean island basalts: Characterization of mantle source reservoirs. *Reviews in Mineralogy and Geochemistry*, *47*(1), 247–317. <https://doi.org/10.2138/rmg.2002.47.8>
- Grassi, D., Schmidt, M. W., & Günther, D. (2012). Element partitioning during carbonated pelite melting at 8, 13, and 22 GPa and the sediment signature in the EM mantle components. *Earth and Planetary Science Letters*, *327–328*, 84–96. <https://doi.org/10.1016/j.epsl.2012.01.023>
- Hart, S. R. (1984). A large-scale isotope anomaly in the Southern Hemisphere mantle. *Nature*, *309*(5971), 753–757. <https://doi.org/10.1038/309753a0>
- Huang, J., Li, S.-G., Xiao, Y., Ke, S., Li, W.-Y., & Tian, Y. (2015). Origin of low $\delta^{26}\text{Mg}$ Cenozoic basalts from South China Block and their geodynamic implications. *Geochimica et Cosmochimica Acta*, *164*, 298–317. <https://doi.org/10.1016/j.gca.2015.04.054>

- Huang, J., Zhang, X.-C., Chen, S., Tang, L., Wörner, G., Yu, H., & Huang, F. (2018). Zinc isotopic systematics of Kamchatka-Aleutian arc magmas controlled by mantle melting. *Geochimica et Cosmochimica Acta*, 238, 85–101. <https://doi.org/10.1016/j.gca.2018.07.012>
- Huang, K.-J., Teng, F.-Z., Elsenouy, A., Li, W.-Y., & Bao, Z.-Y. (2013). Magnesium isotopic variations in loess: Origins and implications. *Earth and Planetary Science Letters*, 374, 60–70. <https://doi.org/10.1016/j.epsl.2013.05.010>
- Inglis, E. C., Debret, B., Burton, K. W., Millet, M.-A., Pons, M.-L., Dale, C. W., et al. (2017). The behavior of iron and zinc stable isotopes accompanying the subduction of mafic oceanic crust: A case study from Western Alpine ophiolites. *Geochemistry, Geophysics, Geosystems*, 18(7), 2562–2579. <https://doi.org/10.1002/2016gc006735>
- Jin, Q.-Z., Huang, J., Liu, S.-C., & Huang, F. (2020). Magnesium and zinc isotope evidence for recycled sediments and oceanic crust in the mantle sources of continental basalts from Eastern China. *Lithos*, 370–371, 370–371. <https://doi.org/10.1016/j.lithos.2020.105627>
- Kelemen, P. B., & Manning, C. E. (2015). Reevaluating carbon fluxes in subduction zones, what goes down, mostly comes up. *Proceedings of the National Academy of Sciences of the United States of America*, 112(30), E3997–E4006. <https://doi.org/10.1073/pnas.1507889112>
- Kirchenbaur, M., & Münker, C. (2015). The behavior of the extended HFSE group (Nb, Ta, Zr, Hf, W, Mo) during the petrogenesis of mafic K-rich lavas: The eastern Mediterranean case. *Geochimica et Cosmochimica Acta*, 165, 178–199. <https://doi.org/10.1016/j.gca.2015.05.030>
- Le Bas, M. J., Le Maitre, R. W., Streckeisen, A., & Zanettin, B. A. (1986). Chemical classification of volcanic rocks based on the total alkali-silica diagram. *Journal of Petrology*, 27(3), 745–750. <https://doi.org/10.1093/ptrology/27.3.745>
- Lee, C.-T. A., Jiang, H., Dasgupta, R., & Torres, M. (2019). A framework for understanding whole-Earth carbon cycling. In B. N. Orcutt, I. Daniel, & R. Dasgupta (Eds.), *Deep carbon: Past to present* (pp. 313–357). Cambridge University Press.
- Lee, C.-T. A., Shen, B., Slotnick, B. S., Liao, K., Dickens, G. R., Yokoyama, Y., et al. (2012). Continental arc-island arc fluctuations, growth of crustal carbonates, and long-term climate change. *Geosphere*, 9(1), 21–36. <https://doi.org/10.1130/ges00822.1>
- Le Roux, V., Lee, C.-T. A., & Turner, S. J. (2010). Zn/Fe systematics in mafic and ultramafic systems: Implications for detecting major element heterogeneities in the Earth's mantle. *Geochimica et Cosmochimica Acta*, 74(9), 2779–2796. <https://doi.org/10.1016/j.gca.2010.02.004>
- Li, S.-G., Yang, W., Ke, S., Meng, X., Tian, H., Xu, L., et al. (2017). Deep carbon cycles constrained by a large-scale mantle Mg isotope anomaly in Eastern China. *National Science Review*, 4(1), 111–120. <https://doi.org/10.1093/nsr/nww070>
- Li, W.-Y., Teng, F.-Z., Ke, S., Rudnick, R. L., Gao, S., Wu, F.-Y., & Chappell, B. W. (2010). Heterogeneous magnesium isotopic composition of the upper continental crust. *Geochimica et Cosmochimica Acta*, 74(23), 6867–6884. <https://doi.org/10.1016/j.gca.2010.08.030>
- Little, S. H., Vance, D., McManus, J., & Severmann, S. (2016). Key role of continental margin sediments in the oceanic mass balance of Zn and Zn isotopes. *Geology*, 44(3), 207–210. <https://doi.org/10.1130/g37493.1>
- Liu, S.-A., & Li, S.-G. (2019). Tracing the deep carbon cycle using metal stable isotopes: Opportunities and challenges. *Engineering*, 5, 448–457. <https://doi.org/10.1016/j.eng.2019.03.007>
- Liu, S.-A., Liu, P.-P., Lv, Y., Wang, Z.-Z., & Dai, J.-G. (2019). Cu and Zn isotope fractionation during oceanic alteration: Implications for Oceanic Cu and Zn cycles. *Geochimica et Cosmochimica Acta*, 257, 191–205. <https://doi.org/10.1016/j.gca.2019.04.026>
- Liu, S.-A., Qu, Y.-R., Wang, Z.-Z., Li, M.-L., Yang, C., & Li, S.-G. (2022). The fate of subducting carbon tracked by Mg and Zn isotopes: A review and new perspectives. *Earth-Science Reviews*, 228, 104010. <https://doi.org/10.1016/j.earscirev.2022.104010>
- Liu, S.-A., Wang, Z.-Z., Li, S.-G., Huang, J., & Yang, W. (2016). Zinc isotope evidence for a large-scale carbonated mantle beneath Eastern China. *Earth and Planetary Science Letters*, 444, 169–178. <https://doi.org/10.1016/j.epsl.2016.03.051>
- Liu, S.-A., Wu, H., Shen, S.-z., Jiang, G., Zhang, S., Lv, Y., et al. (2017). Zinc isotope evidence for intensive magmatism immediately before the end-Permian mass extinction. *Geology*, 45(4), 343–346. <https://doi.org/10.1130/g38644.1>
- Liu, X. M., Kah, L. C., Knoll, A. H., Cui, H., Kaufman, A. J., Shahar, A., & Hazen, R. M. (2016). Tracing Earth's O₂ evolution using Zn/Fe ratios in marine carbonates. *Geochemical Perspectives Letters*, 2(1), 24–34. <https://doi.org/10.7185/geochemlet.1603>
- Lustrino, M., Duggen, S., & Rosenberg, C. L. (2011). The central-western Mediterranean: Anomalous igneous activity in an anomalous collisional tectonic setting. *Earth-Science Reviews*, 104(1–3), 1–40. <https://doi.org/10.1016/j.earscirev.2010.08.002>
- Lustrino, M., & Wilson, M. (2007). The circum-Mediterranean anorogenic Cenozoic igneous province. *Earth-Science Reviews*, 81(1–2), 1–65. <https://doi.org/10.1016/j.earscirev.2006.09.002>
- Maréchal, C. N., Nicolas, E., Douchet, C., & Albarède, F. (2000). Abundance of zinc isotopes as a marine biogeochemical tracer. *Geochemistry, Geophysics, Geosystems*, 1(5). <https://doi.org/10.1029/1999gc000029>
- Maréchal, C. N., Télouk, P., & Albarède, F. (1999). Precise analysis of copper and zinc isotopic compositions by plasma-source mass spectrometry. *Chemical Geology*, 156(1–4), 251–273. [https://doi.org/10.1016/S0009-2541\(98\)00191-0](https://doi.org/10.1016/S0009-2541(98)00191-0)
- Mason, E., Edmonds, M., & Turchyn, A. V. (2017). Remobilization of crustal carbon may dominate volcanic arc emissions. *Science*, 357(6348), 290–294. <https://doi.org/10.1126/science.aan5049>
- McCoy-West, A. J., Fitton, J. G., Pons, M.-L., Inglis, E. C., & Williams, H. M. (2018). The Fe and Zn isotope composition of deep mantle source regions: Insights from Baffin Island picrites. *Geochimica et Cosmochimica Acta*, 238, 542–562. <https://doi.org/10.1016/j.gca.2018.07.021>
- McDonough, W. F., & Sun, S.-s. (1995). The composition of the Earth. *Chemical Geology*, 120(3–4), 223–253. [https://doi.org/10.1016/0009-2541\(94\)00140-4](https://doi.org/10.1016/0009-2541(94)00140-4)
- Minissale, A. (2004). Origin, transport, and discharge of C₀₂ in central Italy. *Earth-Science Reviews*, 66(1–2), 89–141. <https://doi.org/10.1016/j.earscirev.2003.09.001>
- Moynier, F., Vance, D., Fujii, T., & Savage, P. (2017). The isotope geochemistry of zinc and copper. *Reviews in Mineralogy and Geochemistry*, 82(1), 543–600. <https://doi.org/10.2138/rmg.2017.82.13>
- Oppenheimer, C., Fischer, T. P., & Scaillet, B. (2014). Volcanic degassing: Process and impact. In H. D. Holland & K. K. Turekian (Eds.), *Treatise on geochemistry* (2nd ed.) (pp. 111–179). Elsevier. <https://doi.org/10.1016/B978-0-08-095975-7.00304-1>
- Panza, G. F., Peccerillo, A., Aoudia, A., & Farina, B. (2007). Geophysical and petrological modeling of the structure and composition of the crust and upper mantle in complex geodynamic settings: The Tyrrhenian Sea and surroundings. *Earth-Science Reviews*, 80(1–2), 1–46. <https://doi.org/10.1016/j.earscirev.2006.08.004>
- Panza, G. F., Raykova, R. B., Carminati, E., & Doglioni, C. (2007). Upper mantle flow in the western Mediterranean. *Earth and Planetary Science Letters*, 257(1–2), 200–214. <https://doi.org/10.1016/j.epsl.2007.02.032>
- Pichat, S., Douchet, C., & Albarède, F. (2003). Zinc isotope variations in deep-sea carbonates from the eastern equatorial Pacific over the last 175 ka. *Earth and Planetary Science Letters*, 210(1–2), 167–178. [https://doi.org/10.1016/s0012-821x\(03\)00106-7](https://doi.org/10.1016/s0012-821x(03)00106-7)
- Piromallo, C., & Morelli, A. (2003). P wave tomography of the mantle under the Alpine-Mediterranean area. *Journal of Geophysical Research: Solid Earth*, 108(B2). <https://doi.org/10.1029/2002jb001757>
- Plank, T. (2014). The chemical composition of subducting sediments. In H. D. Holland & K. K. Turekian (Eds.), *Treatise on geochemistry* (2nd ed.) (pp. 607–629). Elsevier. <https://doi.org/10.1016/B978-0-08-095975-7.00319-3>
- Plank, T., & Manning, C. E. (2019). Subducting carbon. *Nature*, 574(7778), 343–352. <https://doi.org/10.1038/s41586-019-1643-z>

- Prelević, D., Akal, C., Foley, S. F., Romer, R. L., Stracke, A., & Van Den Bogaard, P. (2012). Ultrapotassic mafic rocks as geochemical proxies for post-collisional dynamics of orogenic lithospheric mantle: The case of Southwestern Anatolia, Turkey. *Journal of Petrology*, 53(5), 1019–1055. <https://doi.org/10.1093/petrology/egs008>
- Prelević, D., Akal, C., Romer, R. L., Mertz-Kraus, R., & Helvac, C. (2015). Magmatic response to slab tearing: Constraints from the Afyon alkaline volcanic complex, Western Turkey. *Journal of Petrology*, 56(3), 527–562. <https://doi.org/10.1093/petrology/egv008>
- Prelević, D., & Foley, S. F. (2007). Accretion of arc-oceanic lithospheric mantle in the Mediterranean: Evidence from extremely high-Mg olivines and Cr-rich spinel inclusions in lamproites. *Earth and Planetary Science Letters*, 256(1–2), 120–135. <https://doi.org/10.1016/j.epsl.2007.01.018>
- Prelević, D., Foley, S. F., Cvetković, V., & Romer, R. L. (2004). The analcime problem and its impact on the geochemistry of ultrapotassic rocks from Serbia. *Mineralogical Magazine*, 68(4), 633–648. <https://doi.org/10.1180/0026461046840209>
- Prelević, D., Foley, S. F., Romer, R., & Conticelli, S. (2008). Mediterranean Tertiary lamproites derived from multiple source components in postcollisional geodynamics. *Geochimica et Cosmochimica Acta*, 72(8), 2125–2156. <https://doi.org/10.1016/j.gca.2008.01.029>
- Prelević, D., Foley, S. F., Romer, R. L., Cvetković, V., & Downes, H. (2005). Tertiary ultrapotassic volcanism in Serbia: Constraints on petrogenesis and mantle source characteristics. *Journal of Petrology*, 46(7), 1443–1487. <https://doi.org/10.1093/petrology/egi022>
- Prelević, D., Jacob, D. E., & Foley, S. F. (2013). Recycling plus: A new recipe for the formation of Alpine-Himalayan orogenic mantle lithosphere. *Earth and Planetary Science Letters*, 362, 187–197. <https://doi.org/10.1016/j.epsl.2012.11.035>
- Qu, Y.-R., Liu, S.-A., Wu, H., Li, M.-L., & Tian, H.-C. (2022). Tracing carbonate dissolution in subducting sediments by zinc and magnesium isotopes. *Geochimica et Cosmochimica Acta*, 319, 56–72. <https://doi.org/10.1016/j.gca.2021.12.020>
- Richter, F. M., Watson, E. B., Mendybaev, R. A., Teng, F.-Z., & Janney, P. E. (2008). Magnesium isotope fractionation in silicate melts by chemical and thermal diffusion. *Geochimica et Cosmochimica Acta*, 72(1), 206–220. <https://doi.org/10.1016/j.gca.2007.10.016>
- Ritter, X., Sanchez-Valle, C., Sator, N., Desmaele, E., Guignot, N., King, A., et al. (2020). Density of hydrous carbonate melts under pressure, compressibility of volatiles and implications for carbonate melt mobility in the upper mantle. *Earth and Planetary Science Letters*, 533, 116043. <https://doi.org/10.1016/j.epsl.2019.116043>
- Robinson, A. H. F. (2002). Overview of the genesis and emplacement of Mesozoic ophiolites in the eastern Mediterranean Tethyan region. *Lithos*, 65(1–2), 1–67. [https://doi.org/10.1016/S0024-4937\(02\)00160-3](https://doi.org/10.1016/S0024-4937(02)00160-3)
- Shu, Z.-T., Liu, S.-A., Prelević, D., Wang, Y., Foley, S. F., Cvetković, V., & Li, S. (2022). Mg and Zn isotopic data and supplementary information for "Recycled carbonate-bearing silicate sediments in the sources of circum-Mediterranean K-rich lavas: Evidence from Mg-Zn isotopic decoupling." <https://doi.org/10.5281/zenodo.7420592>
- Sokol, K., Prelević, D., Romer, R. L., Božović, M., van den Bogaard, P., Stefanova, E., et al. (2020). Cretaceous ultrapotassic magmatism from the Sava-Vardar Zone of the Balkans. *Lithos*, 354–355, 105268. <https://doi.org/10.1016/j.lithos.2019.105268>
- Sossi, P. A., Halverson, G. P., Nebel, O., & Eggins, S. M. (2015). Combined separation of Cu, Fe, and Zn from rock matrices and improved analytical protocols for stable isotope determination. *Geostandards and Geoanalytical Research*, 39(2), 129–149. <https://doi.org/10.1111/j.1751-908X.2014.00298.x>
- Sossi, P. A., Nebel, O., O'Neill, H. S. C., & Moynier, F. (2018). Zinc isotope composition of the Earth and its behavior during planetary accretion. *Chemical Geology*, 477, 73–84. <https://doi.org/10.1016/j.chemgeo.2017.12.006>
- Sun, S. S., & McDonough, W. F. (1989). Chemical and isotopic systematics of oceanic basalts: Implications for mantle composition and processes. *Geological Society, London, Special Publications*, 42(1), 313–345. <https://doi.org/10.1144/gsl.sp.1989.042.01.19>
- Sun, Y., Teng, F.-Z., Pang, K.-N., Ying, J.-F., & Kuehner, S. (2021). Multistage mantle metasomatism deciphered by Mg-Sr-Nd-Pb isotopes in the Leucite Hills lamproites. *Contributions to Mineralogy and Petrology*, 176(6), 45. <https://doi.org/10.1007/s00410-021-01801-9>
- Sweere, T. C., Dickson, A. J., Jenkyns, H. C., Porcelli, D., Elrick, M., van den Boorn, S. H. J. M., & Henderson, G. M. (2018). Isotopic evidence for changes in the zinc cycle during Oceanic Anoxic Event 2 (Late Cretaceous). *Geology*, 46(5), 463–466. <https://doi.org/10.1130/g40226.1>
- Tappe, S., Foley, S. F., Jenner, G. A., Heaman, L. M., Kjarsgaard, B. A., Romer, R. L., et al. (2006). Genesis of ultramafic lamprophyres and carbonatites at Aillik Bay, Labrador: A consequence of incipient lithospheric thinning beneath the North Atlantic Craton. *Journal of Petrology*, 47(7), 1261–1315. <https://doi.org/10.1093/petrology/egl008>
- Teng, F.-Z. (2017). Magnesium isotope geochemistry. *Reviews in Mineralogy and Geochemistry*, 82(1), 219–287. <https://doi.org/10.2138/rmg.2017.82.7>
- Teng, F.-Z., Li, W.-Y., Ke, S., Marty, B., Dauphas, N., Huang, S., et al. (2010). Magnesium isotopic composition of the Earth and chondrites. *Geochimica et Cosmochimica Acta*, 74(14), 4150–4166. <https://doi.org/10.1016/j.gca.2010.04.019>
- Teng, F.-Z., Wadhwa, M., & Helz, R. T. (2007). Investigation of magnesium isotope fractionation during basalt differentiation: Implications for a chondritic composition of the terrestrial mantle. *Earth and Planetary Science Letters*, 261(1–2), 84–92. <https://doi.org/10.1016/j.epsl.2007.06.004>
- Tommasini, S., Avanzinelli, R., & Conticelli, S. (2011). The Th/La and Sm/La conundrum of the Tethyan realm lamproites. *Earth and Planetary Science Letters*, 301(3–4), 469–478. <https://doi.org/10.1016/j.epsl.2010.11.023>
- Vance, D., Little, S. H., Archer, C., Cameron, V., Andersen, M. B., Rijkkenberg, M. J. A., & Lyons, T. W. (2016). The oceanic budgets of nickel and zinc isotopes: The importance of sulfidic environments as illustrated by the Black Sea. *Philosophical Transactions of the Royal Society A*, 374(2081), 20150294. <https://doi.org/10.1098/rsta.2015.0294>
- Wang, S.-J., Teng, F.-Z., Li, S.-G., & Hong, J.-A. (2014). Magnesium isotopic systematics of mafic rocks during continental subduction. *Geochimica et Cosmochimica Acta*, 143, 34–48. <https://doi.org/10.1016/j.gca.2014.03.029>
- Wang, S.-J., Teng, F.-Z., Rudnick, R. L., & Li, S.-G. (2015). The behavior of magnesium isotopes in low-grade metamorphosed mudrocks. *Geochimica et Cosmochimica Acta*, 165, 435–448. <https://doi.org/10.1016/j.gca.2015.06.019>
- Wang, Y., Foley, S. F., Buhre, S., Soldner, J., & Xu, Y. (2021). Origin of potassic postcollisional volcanic rocks in young, shallow, blueschist-rich lithosphere. *Science Advances*, 7(29), eabc0291. <https://doi.org/10.1126/sciadv.abc0291>
- Wang, Y., Foley, S. F., & Prelević, D. (2017). Potassium-rich magmatism from a phlogopite-free source. *Geology*, 45(5), 467–470. <https://doi.org/10.1130/g38691.1>
- Wang, Z. X., Liu, S.-A., Li, S., Liu, D., & Liu, J. (2022). Linking deep CO₂ outgassing to cratonic destruction. *National Science Review*, 9(6), nwac001. <https://doi.org/10.1093/nsr/nwac001>
- Wang, Z.-Z., & Liu, S.-A. (2021). Evolution of intraplate alkaline to tholeiitic basalts via interaction between carbonated melt and lithospheric mantle. *Journal of Petrology*, 62(4). <https://doi.org/10.1093/petrology/egab025>
- Wang, Z.-Z., Liu, S.-A., Chen, L.-H., Li, S.-G., & Zeng, G. (2018). Compositional transition in natural alkaline lavas through silica-undersaturated melt-lithosphere interaction. *Geology*, 46(9), 771–774. <https://doi.org/10.1130/g45145.1>
- Wang, Z.-Z., Liu, S.-A., Liu, J., Huang, J., Xiao, Y., Chu, Z.-Y., et al. (2017). Zinc isotope fractionation during mantle melting and constraints on the Zn isotope composition of Earth's upper mantle. *Geochimica et Cosmochimica Acta*, 198, 151–167. <https://doi.org/10.1016/j.gca.2016.11.014>

- Werner, C., Fischer, T. P., Aiuppa, A., Edmonds, M., Cardellini, C., Carn, S., et al. (2019). Carbon dioxide emissions from subaerial volcanic regions: Two decades in review. In B. N. Orcutt, I. Daniel, & R. Dasgupta (Eds.), *Deep carbon: Past to present* (pp. 188–236). Cambridge University Press.
- Wilson, M. (1989). *Igneous petrogenesis: A global tectonic approach*. Unwin Hyman.
- Wimpenny, J., Yin, Q.-Z., Tollstrup, D., Xie, L.-W., & Sun, J. (2014). Using Mg isotope ratios to trace Cenozoic weathering changes: A case study from the Chinese Loess Plateau. *Chemical Geology*, 376, 31–43. <https://doi.org/10.1016/j.chemgeo.2014.03.008>
- Wood, B. J. (1993). Carbon in the core. *Earth and Planetary Science Letters*, 117(3–4), 593–607. [https://doi.org/10.1016/0012-821X\(93\)90105-1](https://doi.org/10.1016/0012-821X(93)90105-1)
- Yang, C., Liu, S.-A., Zhang, L., Wang, Z.-Z., Liu, P.-P., & Li, S.-G. (2021). Zinc isotope fractionation between Cr-spinel and olivine and its implications for chromite crystallization during magma differentiation. *Geochimica et Cosmochimica Acta*, 313, 277–294. <https://doi.org/10.1016/j.gca.2021.08.005>
- Yang, W., Teng, F.-Z., Zhang, H.-F., & Li, S.-G. (2012). Magnesium isotopic systematics of continental basalts from the North China craton: Implications for tracing subducted carbonate in the mantle. *Chemical Geology*, 328, 185–194. <https://doi.org/10.1016/j.chemgeo.2012.05.018>

References From the Supporting Information

- Hofmann, A. W. (1988). Chemical differentiation of the Earth: The relationship between mantle, continental crust, and oceanic crust. *Earth and Planetary Science Letters*, 90(3), 297–314. [https://doi.org/10.1016/0012-821X\(88\)90132-X](https://doi.org/10.1016/0012-821X(88)90132-X)
- Huang, J., & Xiao, Y. (2016). Mg-Sr isotopes of low- $\delta^{26}\text{Mg}$ basalts tracing recycled carbonate species: Implication for the initial melting depth of the carbonated mantle in Eastern China. *International Geology Review*, 58(11), 1350–1362. <https://doi.org/10.1080/00206814.2016.1157709>
- Ray, J. S., Veizer, J., & Davis, W. J. (2003). C, O, Sr, and Pb isotope systematics of carbonate sequences of the Vindhyan supergroup, India: Age, diagenesis, correlations and implications for global events. *Precambrian Research*, 121(1–2), 103–140. [https://doi.org/10.1016/s0301-9268\(02\)00223-1](https://doi.org/10.1016/s0301-9268(02)00223-1)
- Rudnick, R. L., & Gao, S. (2014). Composition of the continental crust. In H. D. Holland, & K. K. Turekian (Eds.), *Treatise on geochemistry* (2nd ed., pp. 1–51). Elsevier. <https://doi.org/10.1016/B978-0-08-095975-7.00301-6>
- Taylor, S. R., & McLennan, S. M. (1985). The continental crust: Its composition and evolution. *The Journal of Geology*, 94(4), 57–72. <https://doi.org/10.1086/629067>
- Workman, R. K., & Hart, S. R. (2005). Major and trace element composition of the depleted MORB mantle (DMM). *Earth and Planetary Science Letters*, 231(1–2), 53–72. <https://doi.org/10.1016/j.epsl.2004.12.005>